

# **AN INVESTIGATION INTO THE REMOVAL OF OXIDE FILMS FROM MOLTEN A20X WITH THE USE OF ROTARY IMPELLOR DEGASSING**

Thomas Greenwood

A thesis submitted to the University of Birmingham for the degree of MASTER OF  
RESEARCH

**School of Metallurgy and Materials**

**The University of Birmingham**

**Faculty of Engineering**

**August 2012**

UNIVERSITY OF  
BIRMINGHAM

**University of Birmingham Research Archive**

**e-theses repository**

This unpublished thesis/dissertation is copyright of the author and/or third parties. The intellectual property rights of the author or third parties in respect of this work are as defined by The Copyright Designs and Patents Act 1988 or as modified by any successor legislation.

Any use made of information contained in this thesis/dissertation must be in accordance with that legislation and must be properly acknowledged. Further distribution or reproduction in any format is prohibited without the permission of the copyright holder.

# Acknowledgements

I would like to thank Nick Green at the University of Birmingham for his help in creating this thesis.

Also my thanks go to Martin Wood and Keith Denholm at Grainger and Worrall for facilitating the research.

Finally my thanks go to John Forde and Bill Stott at Aeromet for their help and development of A20X.

# Abstract

This thesis investigates the effect of rotary degassing on the level of oxide film inclusions within an A20X melt and in turn their effect of the flow of A20X through ceramic foam filters. Oxide films have been shown to restrict metal flow through filters placed in running systems of castings causing incomplete and unpredictable filling of the mould cavity.

It was found that increasing the rotor speed and decreasing the gas flow rate of argon through the rotating impellor resulted in removal of oxide films from the melt. This is thought to be a result of the smaller bubble sizes and greater distribution of bubbles through the melt created by the increased rotation speed of the impellor.

It was also found that the use of argon purge gas did not remove significant amounts or grain refining  $\text{TiB}_2$  particles from the A20X melt.

# Contents

1. Introduction.....	6
2. Literature review .....	10
2.1. Grain refining in A20X .....	10
2.1.1. The role of $\text{TiAl}_3$ .....	11
2.1.2. The role of $\text{TiB}_2$ .....	11
2.2. Oxide films.....	14
2.3. Degassing.....	17
2.3.1. Existing degassing practices .....	17
2.3.2. Melt Cleaning .....	18
2.3.3. Particle removal and flotation.....	19
2.3.4. Bubble – particle attachment.....	21
2.4. Cleanliness measurement techniques .....	29
2.5. Literature review summary .....	30
3. Experimental Procedure.....	31
3.1. Equipment .....	31
3.2. Procedure .....	34
3.2.1. Density index readings .....	36
3.2.2. $\text{TiB}_2$ measurement .....	37
4. Results and discussion.....	38
4.1. Cleanliness measurements.....	39
4.1.1. ZS degassing condition; gas pressure 0.0 bar, rotor speed 120 rpm .....	40
4.1.2. ZF degassing condition; gas pressure 0.0 bar, rotor speed 600 rpm .....	44
4.1.3. LS degassing condition; gas pressure 0.3 bar, rotor speed 120 rpm .....	47
4.1.4. LF degassing condition; gas pressure 0.3 bar, rotor speed 600 rpm .....	50
4.1.5. HS degassing condition; gas pressure 1.2 bar, rotor speed 120 rpm.....	53
4.1.6. HF degassing condition; gas pressure 1.2 bar, rotor speed 600 rpm.....	56
4.2. Comparisons – Characterisation figure .....	59
4.3. Bubble – oxide film interaction .....	61
4.4. Unstable degassing conditions – possible causes .....	64

4.5. Experimental errors.....	66
4.6. Filter Analysis.....	67
4.7. $\text{TiB}_2$ removal .....	69
4.8. Density index readings (DI) .....	71
5. Conclusions.....	74
6. References.....	75

# 1. Introduction

The automotive industry is continuously developing vehicles with greater performance and increased fuel efficiencies. Two prominent methods being used to achieve this are 1; to increase pressures and temperatures during the combustion of fuel and 2; to decrease the weight of the vehicle. Manufacture of cylinder heads and cylinder blocks in materials with greater strength and thermal conductivity allow for engine re-designs that satisfy both of the above requirements.

Currently design requirements are reaching the limits of what most conventional cast aluminium alloys can offer in terms of strength, fatigue resistance and thermal conductivity. A common alternative to aluminium is cast irons. Cast irons however, have significantly lower thermal conductivities than aluminium alloys. Although cast irons have higher strengths than aluminium alloys at a given temperature, the lower thermal conductivity leads to less heat dissipation after the combustion of fuel. This will often lead to a higher temperature in the stressed areas of cylinder blocks and heads, around the combustion chambers. Depending on the design of the component, the strength can be reduced (due to the increase in temperature) enough to negate the advantage of using cast irons. This, coupled with the greater weight of cast irons compared to aluminium alloys has directed the automotive industry to aluminium alloys for the manufacture of cylinder blocks and heads. (most grey cast irons have thermal conductivities around 45 W/mK whereas most aluminium alloys have thermal conductivities that exceed 115 W/mK).

A20X is an aluminium alloy that has recently been developed by Aeromet and Goodrich (now Aero Engine Controls) in association with the University of Birmingham. It has higher strength

than most common aluminium casting alloys, which makes it attractive to the modern automotive industry.

A20X has similar chemistry and mechanical properties to the A201 system which is one of the strongest cast aluminium alloys to date but has seen limited use due to its susceptibility to hot tearing and unpredictable formation of shrinkage pores. The complex shapes that are required for structural powertrain castings are therefore very difficult to manufacture in A201.

Chemically, A20X is very similar to A201, the main difference being an addition of 4.64 – 4.96 wt% TiB<sub>2</sub> particles added. These lead to a decreased grain size, and significantly alter the feeding characteristics on both a macro and microstructural scale, significantly reducing hot tearing. A20X could therefore be a feasible alloy for complex geometry components.

A20X to date has been developed in the aerospace industry and only virgin ingot has been used for melting and casting. The use of returns (portions of metal that have already been cast) in the automotive industry is essential due to the high cost of virgin ingot.

The flow of A20X through filters appears in line with conventional alloys when using virgin ingot, melted in an induction furnace and cast via a simple melt – degas (using a static or rotating lance) – pour procedure. It is to be noted that this is an observation made in an industrial environment and has not been scientifically measured. Initial casting attempts were made with melts consisting partially of returns. The main problem that revealed itself was that many of the moulds did not fill. Only small amounts of metal would pass through the filters, but in addition to this the weight that did pass through varied greatly with the same equipment set up and melt preparation.

The filters used in these trial castings were 2 back-to-back 30ppi ceramic foam filters from Foseco placed adjacent to the base of the down-sprue at the start of the runner bar. This was



a direct copy of the procedure used in the production of 'aerospace castings' with 20X which appeared to yield the highest and most repeatable mechanical properties from cast sections. The 'aerospace castings' also utilised investment moulds, induction furnaces and virgin ingot.

Sections from the filters of one of these trials were taken for investigation. A layer of oxide films were found bridging the filter pores at the entrance to the first filter. This can be seen in figure 1. A greater density of  $TiB_2$  particles are found upstream of the oxide layer than downstream.

The metal after contains the correct amount of  $TiB_2$  showing that the  $TiB_2$  is able to pass through the filters in reasonable quantities.

It is a fair assumption that the layer of oxide films is restricting the flow of at least the  $TiB_2$  particles through the filters. Therefore the absence of the oxide films bridging between the filter solids may result in greater metal flow through the filters.

Oxide films are created in the running systems and bushes during pouring but as these are likely to vary a lot with component / foundry / process etc this thesis shall focus on the cleanliness of the metal in the furnace. (For the purpose of this thesis 'cleanliness' shall refer to the level of oxide films within the bulk material).

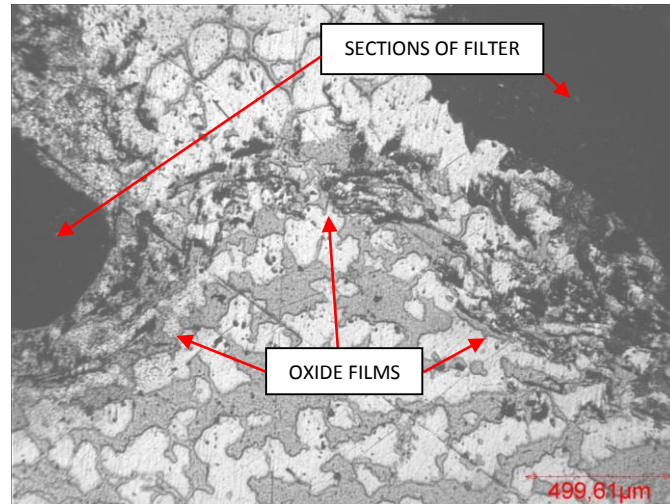


*Figure 1. A micrograph of a section taken through the entrance to a 30ppi filter from a trial casting that only partially filled the mould cavity. The direction of metal flow is vertically upwards in the picture. On the left and the right sections of the ceramic filter can be seen (large black areas). Bridging the gap between the sections of ceramic a layer of several oxide films can be seen.*

In *Figure 1* a layer of several oxide films can be seen bridging the gap between the sections of ceramic. This appears to be intact and is likely to have some tensile strength in the horizontal direction (in the picture) as the bridge has not been washed away by the metal flow but just pushed in the direction of it. It is quite evident that before the filter barrier there is considerably more TiB<sub>2</sub> particles. These can be seen as the medium grey areas between the primary aluminium (very light grey).

## 2. Literature review

### 2.1. Grain refining in A20X

A20X is based on the Al-Cu-Ag (Si - free) system. It shares similar chemical composition with A201 but with the addition of 4.64 – 4.96 wt% TiB<sub>2</sub> particles <sup>1</sup>which appear to give A20X a fully cellular microstructure. This grain structure will alter the feeding mechanisms taking place (Campbell, 2003). Whereas a conventional dendritic alloy will cease to mass feed at around 30% solid, the fully cellular structure found in A20X will continue to mass feed right up to about 95% (J. Forde, pers. Comm., 2011). This change from mostly inter-dendritic feeding to mostly mass feeding for a large portion of the solidification significantly reduces the occurrence of internal shrinkage pores and hot tearing for many geometries. It also offers the advantage of reducing the requirement for ‘chilling’<sup>1</sup> of many components, which has many practical advantages in the foundry.

A20X has been designed to allow for 2 mechanisms of grain refinement to take place; heterogeneous nucleation of  $\alpha$ -aluminium on TiAl<sub>3</sub> particles and TiB<sub>2</sub> particles. There may be evidence that the TiB<sub>2</sub> particles are contributing to the observed reduction in grain size via restricting the growth of the grains; this will be discussed in 2.1.2.

---

<sup>1</sup> ‘Chilling’ is jargon often used in sand foundries. It refers to the act of moulding a solid block of metal into the sand mould to extract heat out of a targeted volume of the solidifying casting. This encourages faster solidification local to the chill (lump of metal) and is used to reduce shrinkage porosity or drive it to an area outside of the final component geometry.

### **2.1.1. The role of $\text{TiAl}_3$**

$\text{TiAl}_3$  particles are often found at the centre of primary aluminium grains in 2D sections of A20X. This would suggest heterogeneous nucleation of primary aluminium is taking place on  $\text{TiAl}_3$  particles. In a review paper Murty et al (2002) summarised that  $\text{TiAl}_3$  is a more potent grain refiner than  $\text{TiB}_2$  or  $\text{AlB}_2$ . The undercooling of the alloy before nucleation of solid  $\alpha$ -aluminium grains is often used as a measure of how potent a grain refiner is (Quested, 2004) as it is an indication of the driving force needed to nucleate a grain, in thermodynamic terms.

Titanium in aluminium undergoes a peritectic reaction at compositions equal to or above 0.15wt%. Therefore, in this composition range the free titanium, dissolved in the liquid aluminium, will form solid  $\text{TiAl}_3$  phases in the melt upon cooling. These will be the first solid to form and on further cooling primary aluminium grains will heterogeneously nucleate on these. Microstructural analysis of A20X shows these particles to be present at the centre of the grains. This grain refining alone would avoid many of the problems created by having in situ solid particles present at melt temperatures (one of which is the subject of this thesis).

### **2.1.2. The role of $\text{TiB}_2$**

$\text{TiB}_2$  particles have been shown to be potential nucleation sites for primary aluminium grains. This is their intended use across the aluminium casting industry. A greater number of  $\text{TiB}_2$  particles with equivalent grain refining efficiencies should nucleate more grains per area leading to a smaller grain size in fully solidified metal. This was the intended use of  $\text{TiB}_2$  particles in the 20X system.

However, current thinking is that dense regions of  $\text{TiB}_2$  particles in A20X are restricting the growth of primary aluminium grains, with a similar result to growth restriction seen in various alloying systems (often referred to as Q) however a different mechanism. This would allow more time for grains to nucleate and therefore a greater density of nucleation sites would lead to a smaller grains size. This is thought because no  $\text{TiB}_2$  particles have been found at the centre of grains but only in the grain boundary regions. A lack of  $\text{TiB}_2$  leads to a larger grain size (authors own work) therefore it must be concluded that they are contributing to a reduction in grain size of the alloy, potentially by restricting the growth of the  $\alpha$ -aluminium grains. This logic is sound however it is not clear if enough work has been done to look for  $\text{TiB}_2$  nucleation sites. With most  $\text{TiB}_2$  particles being  $< 3 \mu\text{m}$  diameter and A20X primary aluminium grains being approximately  $60 - 80 \mu\text{m}$  in diameter, the probability of finding a  $\text{TiB}_2$  particle at the centre of a grain on a 2D section is very low. In addition the presence of  $\text{TiAl}_3$  particles at the centre of most grains does not rule out initial nucleation from  $\text{TiB}_2$  particles. This is supported by the duplex theory which states that  $\text{TiAl}_3$  particles can nucleate themselves off  $\text{TiB}_2$  particles (Mohanty and Gruzleski, 1994). This is current research and has yet to be completed.

Schaffer and Dahle (2005) observed agglomerates of  $\text{TiB}_2$  particles in pure aluminium that had been held molten for an extended period of time. In addition these were found in a settled layer of  $\text{TiB}_2$  particles at the bottom of the melt. This action of agglomerates forming and sinking more quickly than non-agglomerated  $\text{TiB}_2$  could reduce the effective concentration of grain refining particles in the bulk of the melt which in turn may have an effect on grain refining from either nucleation or growth restriction.

The combined effect of providing many potent nucleation sites and the apparent restriction of the growth of  $\alpha$ -aluminium has led to a much smaller grain size. The fine distribution of potent

nucleation sites allows for many grains to nucleate and the restriction of growth allows time for more nuclei to form in the neighbouring volumes of metal leading to more grains per unit volume. The cellular structure of A20X appears to allow for mass feeding up to a much higher percentage solid and virtually eliminates interdendritic porosity.

## 2.2. Oxide films

Oxide films, often also referred to as bifilms in literature, are a common occurrence in cast aluminium. The reactivity of molten aluminium with oxygen is such that aluminium oxide will form on the surface of the molten metal. If these oxide films stay on the surface of the metal they will cause little or no damage to the casting in terms of strength and durability and in fact are the main contributing factor of aluminium's high corrosion resistance. However in the casting process it is near impossible to avoid entrainment of these oxide films into the bulk material. This entrainment results in 2 films meeting each other and as alumina remains solid at all industrial aluminium melt temperatures (melting point of alumina; 2072°C) these will not chemically bond or fuse. This leads to defects that are effectively pre-existing cracks and cause stress concentrations that often lead to failure. This contributes to the scatter in mechanical properties, notably ductility and fatigue resistance that is well known in castings (Dai et al, 2002).

Entrainment of oxide films can happen via the following mechanisms:

- Pre-existing oxide films on the solid charge aluminium that is loaded into the melt can become entrained upon melting.
- Oxide films generated on the surface of the molten aluminium can be entrained due to surface turbulence of the aluminium. This mechanism can be further characterised to the part of the melting and casting procedure where it occurs which has good relation to the thickness of the oxide films.

The temperature of the molten metal dictates the speed at which oxide will be generated. In the Ellingham diagram (*figure 2*) the free energy vs. temperature are plotted. This shows that

the speed of oxidation increases with increasing melt temperature. Aluminium at all molten temperatures will have a rate of production of alumina at its surface therefore the longer this has to form, the thicker this oxide film. A melt holding stage during molten metal preparation will often be the longest time period of oxide formation and can result in thick oxide films > 100  $\mu\text{m}$  thick which have formed over times greater than 10 minutes (ref). These thick oxide films formed before pouring are often referred to as 'old' films.

Thin oxide films are also formed in the pouring and mould filling stage when new molten aluminium is exposed to the air for less than 10 seconds resulting in thinner oxide films  $\sim 1 - 100 \mu\text{m}$ . These are known as 'young' films.

The holding time of the melt during any experimentation may therefore introduce variation and inaccuracy due to the thickening of oxide films. In addition it will be very difficult to control the type and quantity of films that are already present in metal ingots used. This point also illustrates the effect of using recycled aluminium (returns) in any casting activity. The quantity of films in recycled materials will not only be variable but difficult to measure in a cost effective manner. Therefore it is valuable to the foundry to have a cleaning process that can bring molten metal back to a given cleanliness.

It is important to consider the formation of all types of oxide films in each part of the melting, holding and casting stages and how they can be reduced, removed or not entrained. If the young oxide films created during the pouring stage are abundant and of sufficient strength to bridge the filter pores and cause the variation in melt filling that has been observed in 20X then a melt cleaning stage that removes oxide films may be ineffective at promoting consistent flow through filters.



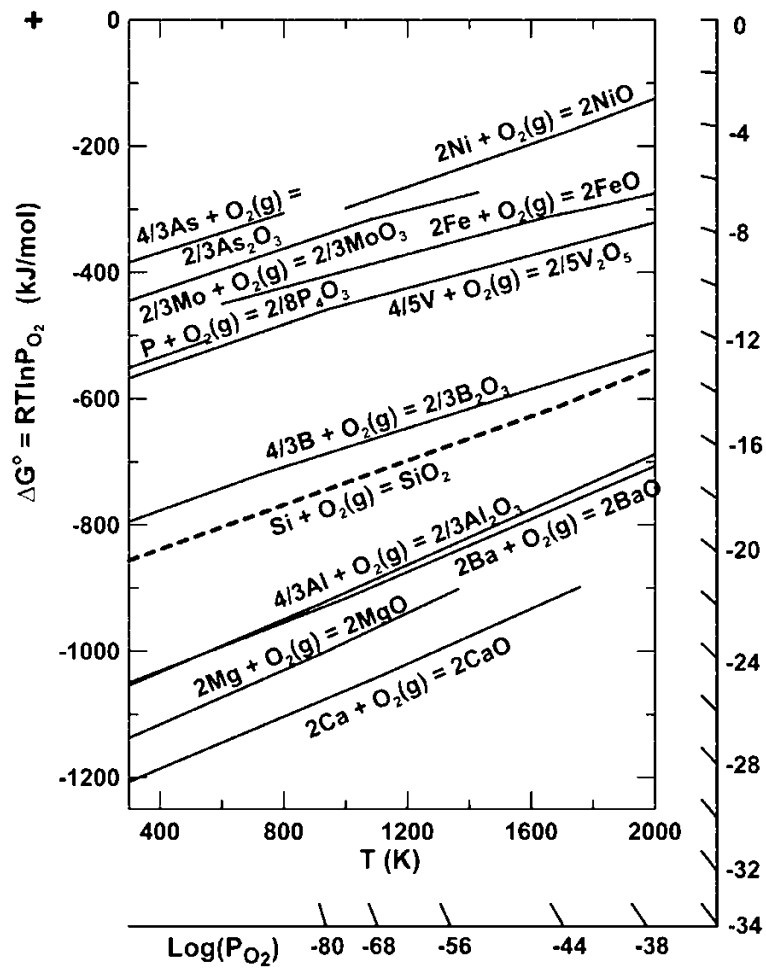


Figure 2. Ellingham diagram for aluminium based oxides.

## 2.3. Degassing

Degassing is an important stage of the melt preparation for any aluminium alloy. Traditionally the primary function is to remove dissolved hydrogen from the liquid aluminium. The solubility of hydrogen in liquid aluminium is much greater than that in the solid and hydrogen will readily dissolve into the melt (Campbell, 2003). Therefore, if the level of hydrogen present in the liquid exceeds the maximum solid solubility then upon solidification it will be rejected and will form pores. These are detrimental to a castings quality.

To remove the hydrogen a degassing stage is introduced into the melt preparation process. This is common place in foundries. There are several methods of this but they all follow similar principals:

A gas that does not readily dissolve in or react with aluminium (most commonly argon) is passed through the melt. The bubbles will have a lower hydrogen content than the melt so diffusion of hydrogen into these bubbles takes place. The bubbles will then reach the top surface of the melt where they will be released into the atmosphere. This is carried out until a hydrogen level lower than the solid solubility is achieved, often with a safety factor added.

### 2.3.1. Existing degassing practices

- Tablet. Tablets are immersed into the melt and will thermally degrade and release gas. These gas bubbles will remove hydrogen from the aluminium (mechanism detailed above). Hexachlorethane tablets were common (Campbell, 2011) however their use is now limited as they release bubbles of chlorine gas which is toxic.
- Lance. This method involves introducing bubbles to the melt via a lance, usually clay graphite. Various gasses could be used with nitrogen and argon being the most

common. This method in its basic form produces large bubbles which will have poor distribution through the melt. This achieve a slow rate of hydrogen removal and entrain oxide films when the large bubbles burst at the surface. It has been improved with the use of porous lances which produce smaller bubbles and can have better distribution around the melt.

- Rotary. Rotary impeller degassing is an improvement to the lance degassing technique. This process still uses a lance to inject bubbles into the bottom of the melt however the lance spins. This shears the bubbles resulting in smaller bubbles and better distribution around the melt. This is common place in todays foundries and shall be the degassing technique utilised in this study.

Variables in the degassing process that may affect the speed of hydrogen removal and also any change in cleanliness may be quantity of melt and the height of the melt above the height of bubble release from the rotor. This will dictate the distance that the bubbles travel through the melt and therefore this may affect the amount of interaction each bubble has with either oxide films of  $TiB_2$  particles.

### **2.3.2. Melt Cleaning**

There are different methods of cleaning the melt; with either gas and/or flux, filtration (which can happen at various locations upstream of the mould cavity) and settling of the metal for extended periods of time (leaving the melt undisturbed so that particles with different densities to the molten alloy can segregate). This thesis will focus on using the degassing stage as a cleaning mechanism and focus on the use of purge bubble without the use of flux.

Degassing presents a cleaning opportunity as the bubbles travelling through the melt may attach to films or particles, carrying them to open upper surface where they can be manually removed.

It is a fair assumption that the removal of oxide films from the melt will have a positive effect on the flow rate and consistency of flow of A20X through filters in castings running systems (based on the information presented in the introduction). It does however present a risk – the degassing stage has the potential of removing  $\text{TiB}_2$  particles (Roy et al, 2001, Warke et al, 2005). The removal of significant quantities of these will reduce the grain refining effect, lead to a larger grain size and hence affect solidification kinetics. In the author's background work with A20X the presence of  $\text{TiB}_2$  (A20X as opposed to A201) has been shown to largely eliminated gross sub-surface shrinkage defects and also significantly improve the hot tear resistance – a major problem in high copper aluminium alloys (2XX series casting alloys).

The good grain refining occurring in A20X also leads to a fully cellular structure in much slower solidifying areas such as large section thicknesses. This gives the opportunity of casting billets that then can be used for 'machined from solid' parts. Although there may be weaker material in the centre of the billet this avoids many of the centre line problems of using thick forged material. This opens up a potential market for A20X to replace machined from solid parts which require a billet of up to around 150mm diameter.

### **2.3.3. Particle removal and flotation**

There have been many studies (Roy et al, 2001. Hewitt et al, 1994. Nguyen et al, 1998. Pyke et al 2003, Shahbazi et al, 2010. Kumar et al, 2009. Zhang and Taniguchi, 2000. Nguyen, 1998) on the removal of particles from flotation cells using rotary impeller gas injection and also specific

removal of grain refiner particles from aluminium melts. Flotation refers to the removal of particles from a solution or suspension via attachment to buoyant bubbles where transport to the surface forms a higher concentration suspension that can be mechanically removed. Flotation has seen much research as it is of specific interest to a several industries, most notably the mineral extraction industry. The general aim of this industry is to remove mineral particles from a solution however an understanding of the science may help when developing a process to remove oxide films but not  $\text{TiB}_2$  particles from A20X.

The studies that relate to the aluminium – ceramic particle systems tend to concentrate on lower levels of grain refining particles than that found in A20X or use SiC particles (it must be considered however that even  $\text{TiB}_2$  particles can be of difference sizes and shapes).

There may be several mechanisms taking place within a degassing system that have the potential to remove small particles from the bulk liquid:

- Settling of the particles – either by sinking as would be expected with  $\text{TiB}_2$  or floating which may be true for  $\text{TiB}_2$  particles that have become attached to oxide films.
- Motion of the liquid aluminium that transports the particles to either the surface of the melt or the crucible walls where they may become trapped. This could happen by, convection or as would be more likely in rotary degassing, flows caused by the rotating impeller.
- Attachment to the gas purge bubbles (flotation) and then subsequent transport to the melt surface where they may become trapped in the films/dross on the surface of the melt.

Warke et al. (2005) uses mathematical models to predict both the removal of particles and hydrogen from aluminium melts with rotary degassing. The majority of the models appear to

focus on the bubble – particle attachment and there is some work of the effect of Stokes flotation but it does not take into account the particle transport via metal flow mechanism. Schaffer and Dahle (2009) concluded that the removal of specifically grain refining particles is not in fact due to flotation at all but the other two mechanisms – sedimentation and transport via flow patterns. In their work however they used a static lance degasser – not a rotary degassing method. The purpose of this was to specifically eliminate the very aggressive stirring associated with rotary degassing. They found that particle removal was just as evident when no gas was passed through the melt and concluded that sedimentation in their case, and turbulence in the case of rotary degassing, was the source of removal. It is possible that their conclusions are flawed as they have not fully addressed the bubble – particle attachment situation. The conditions in lance degassing are highly different from rotary. Most notably the size of the bubbles and the distribution of them throughout the melt will be very different and may lead to a different probability of attachment. Their work does, however, highlight the need to compare particle removal during degassing to a controlled condition where no gas is passed through the melt. In the case of rotary degassing a zero flow rate condition will still have significant turbulence (depending on the speed of rotation).

#### **2.3.4. Bubble – particle attachment**

The literature on bubble – particle attachment (Hewitt et al, 1993, Nguyen et al 1998, Pyke et al, 2003, Shahbazi et al, 2010, Ramirez et al, 1999) suggested that several variables will affect the particle attachment efficiency and the probability of the particle being fully transported to the surface. In identifying these variables it is important to consider the full mechanism of flotation:

In order for flotation to occur bubble-particle collision needs to take place. It is possible that a particle may be transported a small distance via a bubble or multiple bubbles passing in close proximity due to the disturbance of the liquid but it is reasonable to assume this negligible when in the presence of stronger flows created by the rotation of the degassing impeller. If collision does take place and there is contact between the bubble and particle then the length of time that the particle remains attached will dictate the displacement it experiences. There is therefore a probability of attachment and a probability of detachment.

The variables that will limit the probability of attachment are:

- Particle size
- Particle chemistry
- Particle concentration (in the suspension)
- Bubble size
- Bubble chemistry
- Bubble quantity per unit volume
- Melt agitation / turbulence
- Distance between gas injection and melt surface (depth of the melt)

The variables that will influence particle detachment are:

- Particle size
- Particle chemistry
- Bubble size
- Bubble chemistry
- Melt agitation / turbulence
- Distance between gas injection and melt surface (depth of the melt)

With regards to the A20X system all particle related variables are fixed. Bubble chemistry is also fixed – Argon will be used as this is inert. Many foundries use nitrogen gas but this can react with the aluminium leading to unwanted phases. Celik and Doutre (1989) found that use of either pure nitrogen or argon gas was completely ineffective at removing inclusions but a mixture of chlorine and nitrogen would remove inclusions. Of course in the A20X system the aim is to not remove particles but that the bubbles can still physically remove films without perhaps any chemical wetting required. The depth of the melt can be changed but in order replicate the desired production route a standard 300kg capacity pot shall be used and shall be filled at the beginning of the experiments.

Roy et al (2001) suggested that there is an incubation period at the start of degassing where no removal of particles occurs followed by an exponential decrease in particle concentration with time. Attempts were made to minimise the incubation period by altering the chemistry of the gas (changing the chlorine content). Firstly, the system here is different to the A20X system – SiC particles were used. Secondly their method of identifying the incubation period is does not appear sound. The incubation period was characterised by analysing when the level of inclusions dropped below the initial amount added. The error in the measurements meant that in several cases the measured level of inclusions was far higher than the original amount added. Although some of their results do show some lack of inclusion removal at the beginning of the degassing cycle the diagnosis of a completely separate incubation period and removal period is does not appear valid. This however will be kept in mind when reviewing the results of the experiments in this thesis.

Due to many of the variables that can affect bubble-article attachment and detachment being fixed in the case of A20X, the variables that can be altered therefore, are bubble size, bubble quantity and melt agitation / turbulence are the variables available in the A20X degassing set



up. The controls available that will influence these are gas flow rate and rotor speed on the injection impeller.

Regarding bubble size Wu et al (2007) experimented with a water-bubble set up to investigate the influence of the two variables rotor speed and gas flow rate. They found that increasing rotor speed with a constant gas flow rate decreased bubble size and an increase in gas flow rate with a constant rotor speed increased bubble size. The rotor design is likely to have an influence on this so the exact values may not correlate but these general trends should be seen in the A20X system. Based on these findings to achieve the smallest bubble size will involve a fast rotor speed and a low flow rate. To achieve the largest bubble size requires a slow rotor speed and a high flow rate. It is likely however (and evident when viewing the melt surface during degassing), that an increase in rotor speed will increase the level of turbulence within the melt.

Bubble quantity will be influenced by both rotor speed of the impeller and gas flow rate. Obviously the gas flow rate will dictate exactly the total volume of the bubbles being released per unit time but the total amount of bubbles will vary depending on the rotor speed with a constant flow rate as more bubble shearing will take place resulting in smaller volume bubbles. Exact control or measurement of the amount of bubbles is difficult but should be constant for a given degassing condition.

Despite the conclusion by Celik and Dautre (1989) that argon will not remove inclusions, due to the large amount of  $TiB_2$  particles which virtually guarantee collision and the importance of  $TiB_2$  to the A20X system, a degassing cycle should be designed assuming that pure argon bubbles do have the potential to remove particles.

The work by Warke et al (2005) shows that increasing gas flow rate with a constant rotor speed increased the particle removal (*Figure 2*). Combining this with Wu's work suggests that a degassing condition with larger bubble sizes coupled with a greater concentration of bubbles will remove more particles from the melt per unit time. This prediction is valid for a particle size of 3  $\mu\text{m}$  and greater which is approximately the maximum size of the  $\text{TiB}_2$  particles in the A20X system (*Figure 3*). For particles below 3  $\mu\text{m}$  Warke at all predicted almost no removal. They have shown that an increase in gas flow rate does increase the rate at which dissolved hydrogen is removed from the melt. Considering that pure argon should not collect particles, increasing the gas flow rate should therefore not result in particle removal and a shorter degassing cycle can be used to achieve the same hydrogen level. The effect of this on the cleanliness level of the melt is unknown however.

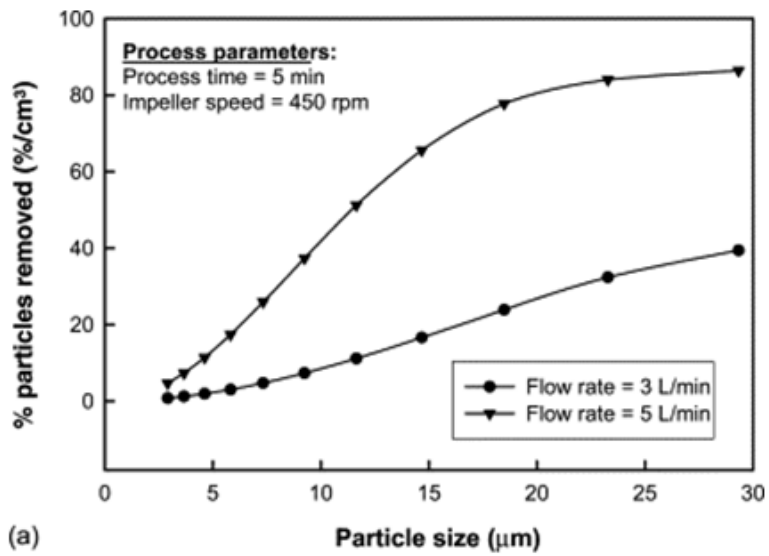


Figure 3. Increasing the flow rate with constant impellor speed will increase the rate of particle removal. Graph taken from Warke et al (2005).

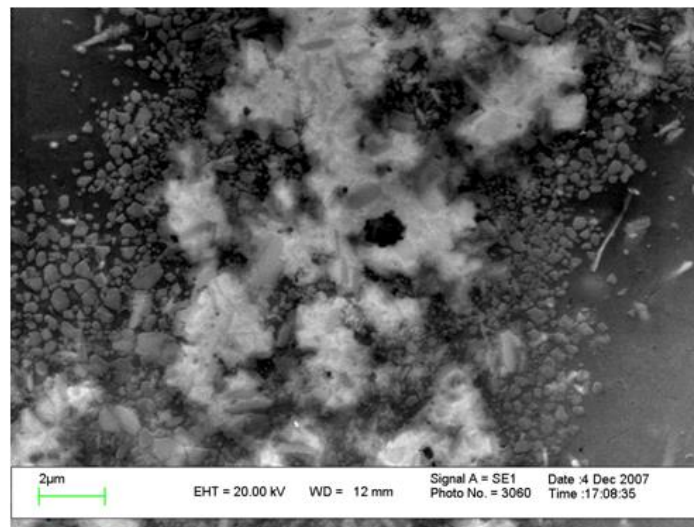


Figure 4. An SEM image of a typical eutectic region / grain boundary in the A20X system. The TiB<sub>2</sub> can be seen as the medium grey blocky particles. Their sizes are approximately 0.2 - 3.0μm. Picture supplied by J. Forde (pers. Comm. 2011).

The work of Warke et al (2005) also identified a small increase in particle removal when increasing impeller speed with a constant gas flow rate (*Figure 4*). In this scenario the size of the bubbles has decreased which given the constant gas flow rate will also increase the number of bubbles. This caused only a very slight increase in particle removal. It is unclear if the smaller bubble size was contributing to a greater particle removal rate or if the greater number of bubbles per unit time is. If there are significantly more bubbles then it may be that small bubbles are in fact less efficient per bubble with regards to particle removal.

Warke's prediction is from a particle population balance equation that gives a change in particle size distribution density with time. They validated their model with an experiment in which aluminium oxide particles were removed from a melt with rotary argon degassing. The remaining particle size distribution was then measure via image analysis of a polished section and showed good correlation to the prediction.

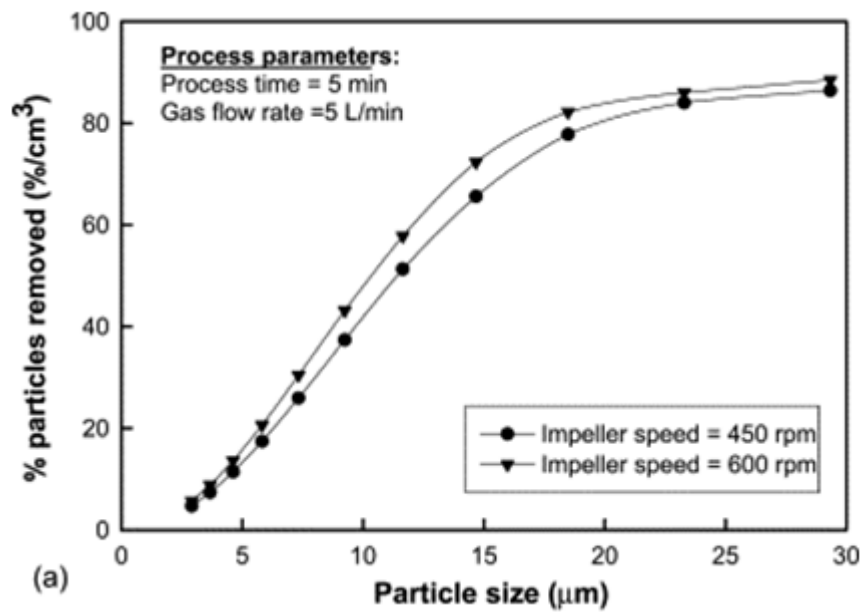


Figure 5. Graph showing an increase in impellor speed with a constant gas flow rate slightly increases particle removal via flotation. Graph taken from Warke et al (2005).

Warke et al (2005) verified their model in two experiments; hydrogen concentration against time for a given flow rate and a fixed impeller speed and particle density against particle size after 20 minutes of degassing with a fixed impeller speed and gas flow rate.

## 2.4. Cleanliness measurement techniques

Several methods for assessing cleanliness of metal exist and are summarised below:

- Metal filtering e.g. PoDFA, LAIS Prefil. These methods involve passing molten metal through a fine filter that will catch all solids above a certain size. The filter and remaining metal can then be sectioned and analysed giving information about the quantity, size distribution and chemistry of inclusions in the melt. The PoDFA and LAIS methods are as described with the LAIS method involving submersing the equipment in the actual melt. Prefil also records the flowrate through the filter which, as the flow rate is reduced by solids that are deposited on the filter, is an additional indication of the metal cleanliness.
- Sample fracture e.g. K-Mold. This method involves fracturing a solidified sample of metal. Most pre-existing solid inclusions will give a stress concentration in the solidified metal. If the metal is fractured it is likely to expose these inclusions on the fracture surface. The K-Mold method is also sensitive to oxide films as these are easily exposed on the fracture surfaces.
- Electric resistance e.g. LiMCA. The LiMCA method measures the electric resistance of the metal sample through a small hole in an insulating material. Metal is forced through the hole and the resistance is altered when an inclusion with a different resistivity to that of the parent metal passes through. The resistance measured is proportional to the size of the inclusion therefore size distributions can be obtained via this method.

## 2.5. Literature review summary

- A larger bubble is more likely to remove a particle than a smaller bubble.
- Argon bubbles should not remove TiB<sub>2</sub> particles.
- Bubble size is decreased by decreasing the gas flow rate through the impellor and increasing the rotation speed of the impellor.

## 3. Experimental Procedure



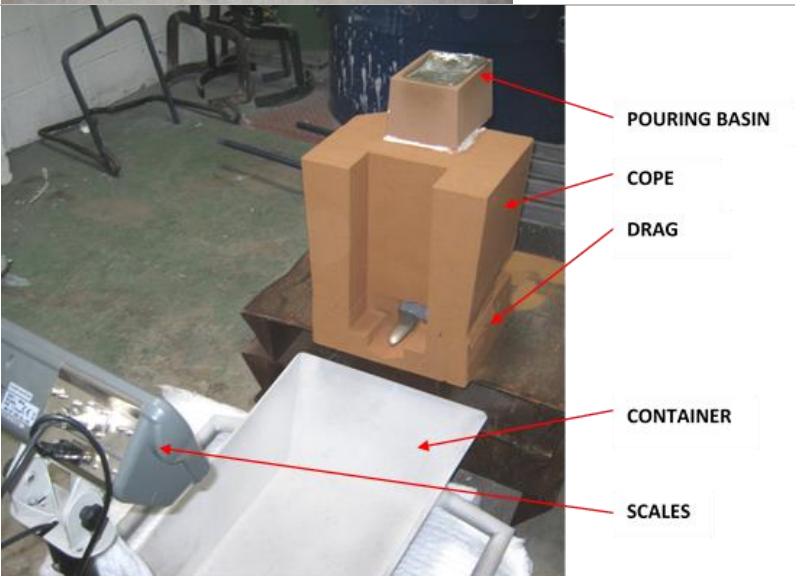
### 3.1. Equipment

Table 1. Equipment list.

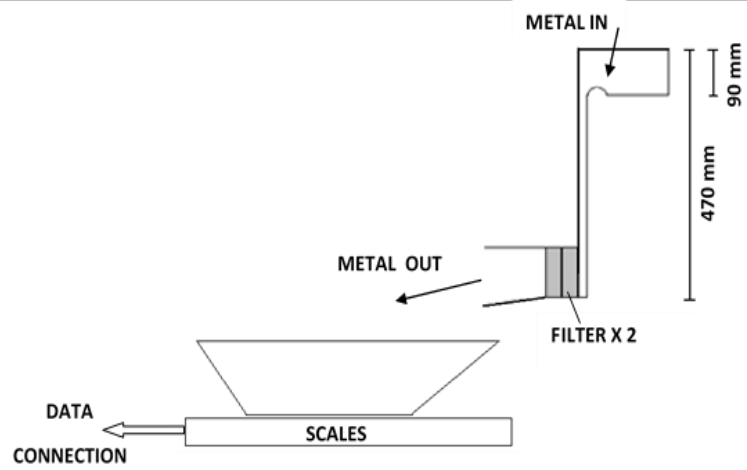
ITEM	DESCRIPTION
A	Electric resistance furnace with clay graphite crucible (aluminium capacity 300kg). Make; Foseco. Model; BU200 ISO
B	Rotary degassing unit. Make; Hepworth minerals and chemicals Ltd. Model; Heproject rotary flux feeder.
C	Transfer ladle. Hand held, 13 kg capacity steel ladle, iron oxide coating.
D	3 part mould – schematic shown below. Silica sand, 2 back-to-back Foseco Sivex 30 ppi ceramic foam filters.
E	Steel container (to receive metal passed though mould
F	Scales with digital output – weight at 1 second intervals. Make; A&D instruments Ltd. Model; AD-4405-EC
G	Density index testing machine; Ideco vac test
H	Chemistry sample die
I	Spectrograph; Hilger analytical



Table 2. Pictures and schematics:

Item	Picture / schematic	Notes
C		
H		
D, E, F		<p>Picture of experimental pouring system. The mould is placed above a steel container that will receive the molten aluminium after it has passed through the mould / filters. The container is placed on scales with a digital output (to log weight against time).</p>

D, E,  
F



Schematic of flow rate  
experiment set up.

## 3.2. Procedure

6 different degassing procedures were investigated and are detailed in *Table 3. Degassing conditions.* below:

*Table 3. Degassing conditions.*

Code	Gas flow rate (achieved by a gas pressure on instrument [bar])	Rotor speed [rpm]	Treatment length [seconds]
ZS	0.0	120	600
ZF	0.0	600	600
LS	0.3	120	600
LF	0.3	600	600
HS	1.2	120	600
HF	1.2	600	600

The following actions were carried out for each degassing condition (*Table 4*):

*Table 4. Procedure.*

Action	Description
1	Between 200 kg and 300 kg of A20X alloy was melted in equipment item A. All metal used was secondary A20X material in large ingots. The metal holding temperature was $810^{\circ}\text{C} \pm 10^{\circ}\text{C}$ .
2	The melt was degassed at the holding temperature of $810^{\circ}\text{C} \pm 10^{\circ}\text{C}$ with equipment item B to a given condition (detailed in table 1)
3	The melt was left undisturbed for 11 minutes $\pm$ 2 minutes. During this time small slugs of metal were taken (with minimal disturbance to the melt) to measure chemistry with equipment item I and gas content (density index) with equipment item G.
4	A sample of molten metal was transferred from the melt to the pouring bush using 1 hand held ladle (equipment item C). Immediately prior to metal transfer the

surface dross was removed and the melt was manually stirred with the ladle. Care was taken to not disturb the melt surface during stirring. Metal samples were between 10 and 13kg. No stopper was placed in the bush therefore filtering and weight measurements started immediately upon pouring. The weight at time intervals of 1 second was recorded using a computer linked to the scales (equipment item F).

**5** Actions 2, 3 and 4 were then repeated 3 additional times for each degassing condition (totalling 4 times per condition). No additional metal was added to the melt.

Actions 1 to 5 were carried out for all degassing conditions detailed in *Table 3*.

All charge metal used was secondary A20X billet. All conformed to the following chemical specification (*Table 5*):

*Table 5. A20X chemical composition.*

Element	Cu	Ag	Mg	Br	Ti	Mn	Si	Fe
Content	3.7 –	0.6 –	0.3 –	1.45 –	3.49 –	0.2 – 0.4	0.10 max	0.05 max
[wt%]	4.0	1.0	0.6	1.55	3.71			

### 3.2.1. Density index readings

The hydrogen content in the metal is indirectly measured via measuring the density index.

Equipment item G was used for this. It involves solidifying 2 samples of metal, one in atmospheric pressure and one in 80mbar pressure. The gas in the metal will form pores that will expand more in the reduced pressure sample during solidification and create a lower density for that sample. The density index reading gives an indication of the total gas content in the metal and is calculated with the following formula:

$$\frac{\rho_{atmospheric} - \rho_{vacuum}}{\rho_{atmospheric}} \times 100$$

Where:

$\rho_{atmospheric}$ : Density of the sample solidified under atmospheric temperature

$\rho_{vacuum}$ : Density of the sample solidified under 80mbar

Not all of the density change will be due to hydrogen porosity and this test does not distinguish between hydrogen and other gasses or inclusions. Haber et al (2009) indicates that there is a linear relationship between hydrogen content and the density index reading at high hydrogen contents however this relationship can break down at low hydrogen contents. This is most likely because of the quantity of oxide films in the sample which will affect the readings as these provide nucleation points for gas pores. It is however an accepted industry standard test and in practice has proved the most robust indication of gas content due to other methods being sensitive to certain composition of small changes in sample size, hence its use in this series.

### 3.2.2. TiB<sub>2</sub> measurement

To measure the quantity of TiB<sub>2</sub> present the most accurate method available shall be to produce a coin sample<sup>2</sup> at the desired point in the process and then perform a spectrometer reading. This will give the weight percent boron within the material. All of the boron will be tied up in TiB<sub>2</sub> particles so this shall be directly proportional to the quantity of TiB<sub>2</sub> particles in the melt.

To date no detailed analysis of the effect of TiB<sub>2</sub> quantity on grain size has been performed. Also there are other variables that will have an effect on grain size, most notably casting temperature.

Area fraction analysis of the eutectic phase would also not provide accurate results as the eutectic is not 100% dense TiB<sub>2</sub> as it contains other phases and some pure aluminium.

---

<sup>2</sup> A coin sample is a small quantity of metal poured into a steel die to force very fast solidification and hence no settling / segregation. This will give accurate representative chemistry throughout the thickness of the sample.

## 4. Results and discussion

The results are separated into the following categories:

1. Cleanliness measurements
  - a. Weight against time graphs displayed with flow rate against time graphs for each degassing condition. All 4 measurements for the individual degassing conditions are displayed on the same graph.
  - b. Flow rate against weight graphs.
  - c. Characterisation figures.
  - d. Filter analysis.
2.  $\text{TiB}_2$  removal – boron content readings from coin samples.
3. Density index readings.

## 4.1. Cleanliness measurements

For each degassing condition weight against time and flow rate against time graphs have been plotted. The zero weight reading 1 second before the first positive weight reading has been plotted at 0 seconds.

The weight against time graphs show the raw data with weight recordings every 1 second.

The flow rate figures are calculated by subtracting each weight reading from the previous, giving the average flow rate over the second preceding each reading.



4.1.1. ZS degassing condition; gas pressure 0.0 bar, rotor speed 120 rpm

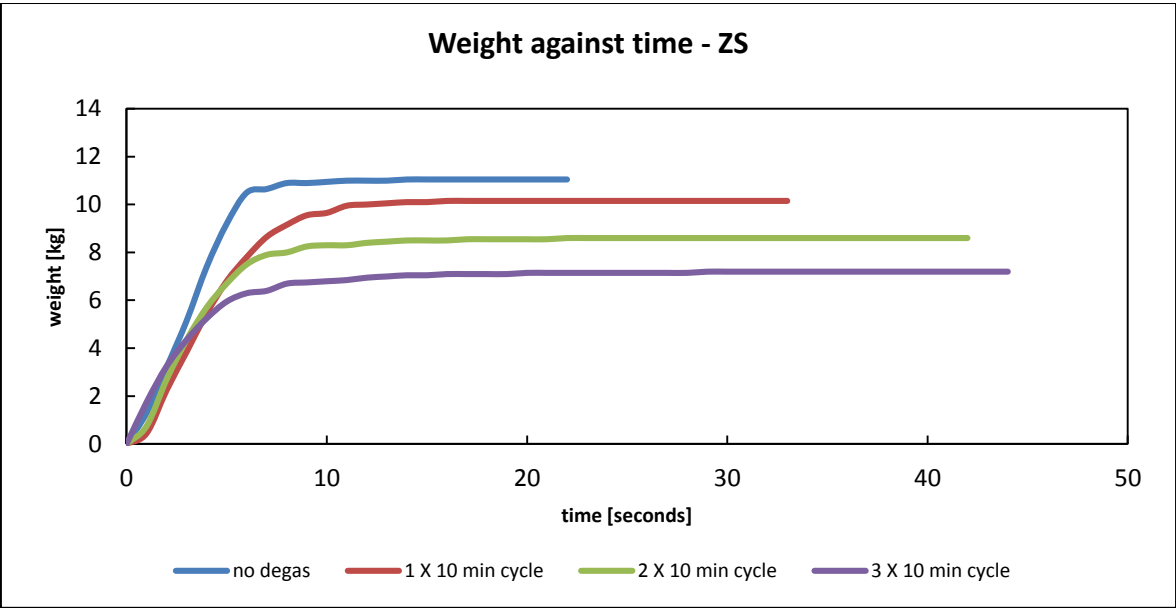


Figure 6. Weight against time - ZS.

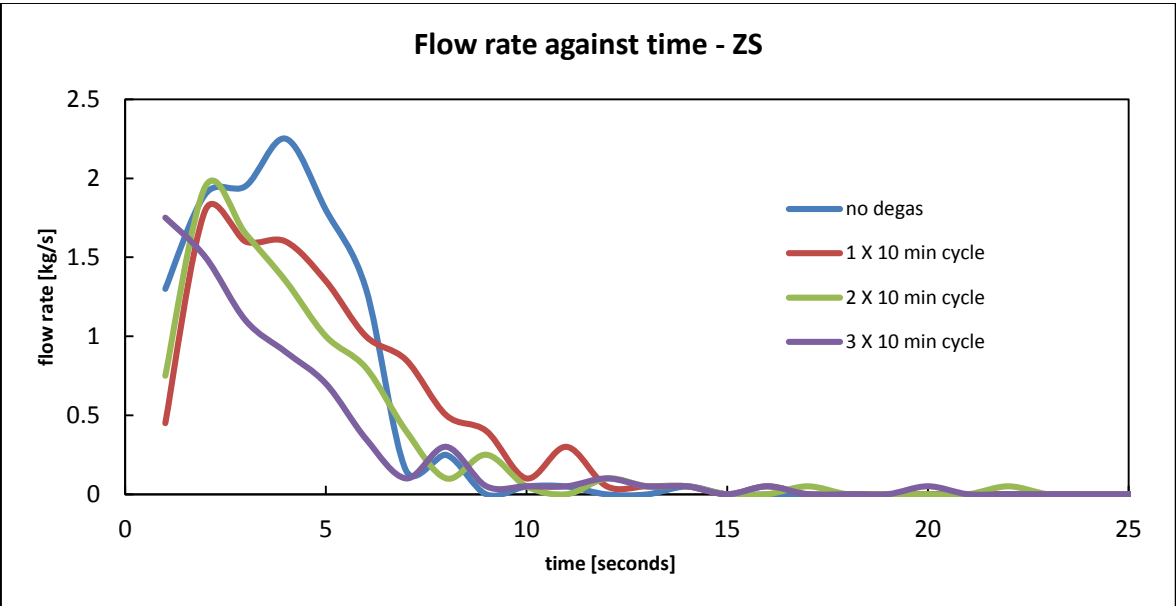


Figure 7. Flow rate against time - ZS.

The zero gas flow rate (0.0 bar gas pressure) and low rotor speed (120 rpm) condition has resulted in a reduced total volume of metal passing through the filters after each successive degassing cycle. In the initial measurement taken before any degassing cycles all of the metal flowed through the filters. The flow rate remained high until the majority of the metal (approximately 9 – 10 kg) had been delivered with the only major drop in flow rate coinciding with the end of metal delivery. This suggests that there were few oxide films that were of a size and strength to get caught in the filter and then impinge metal flow.

In the measurement after the first cycle the full sample passed through the filters but there is a gradual decrease in flow rate with time. This must be due to an increasing impingement of flow through the filters during pouring and may suggest a continuous deposition of oxide films on the filters. The measurements after the second and third cycles showed a similar rate of decrease of flow rate and in both measurements the full sample did not pass through the filter with the least amount of metal passing through on the last measurement, after 30 minutes total cycle time.

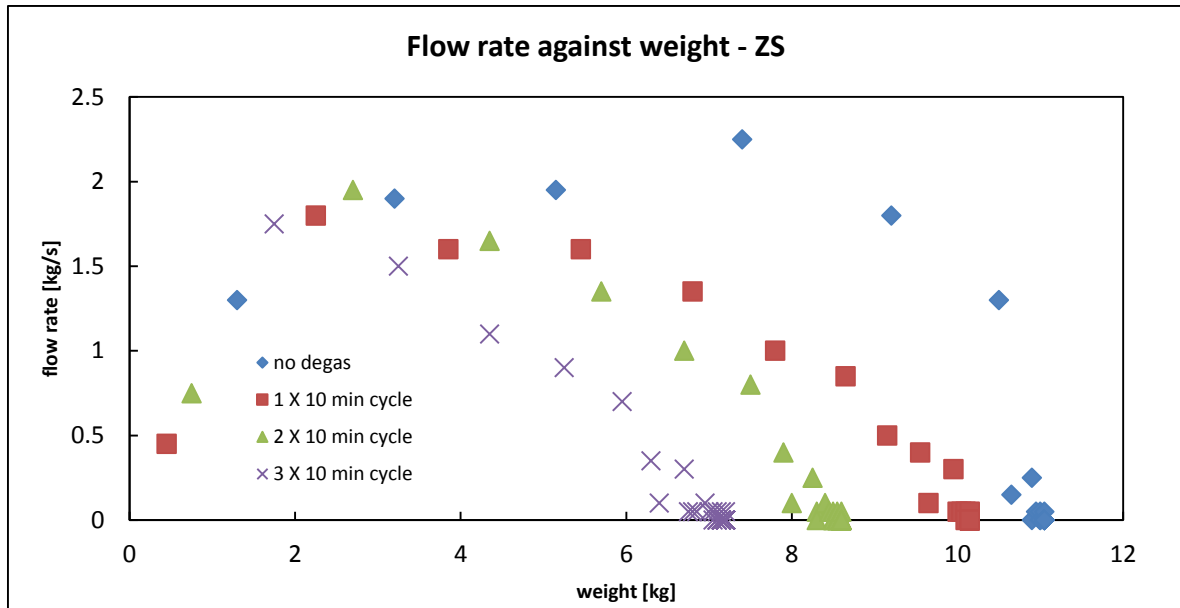


Figure 8. Flow rate against weight - ZS.

The above graph plots flow rate against weight. This should give a reading that represents the restriction of flow through the filter and therefore an indication of the quantity of films that were in the metal delivered up until that data point. This should be advantageous as it is a direct reading of the population density of films within the melt. This representation shows the same trend as the weight against time and flow rate against time graphs with the initial reading retaining a high flow rate throughout the majority of metal delivery. With each successive degassing cycle the negative gradient of the graph increases in magnitude indicating an increase in oxide films within the melt.

In this 'degassing' condition no bubbles pass through the melt so there can be no oxide film removal from bubble – particle interactions. The agitation of the melt with the slow rotation of the impeller appears to have entrained films. If there is removal of the films via deposit of

them on the crucible walls, base or on the surface of the melt then it appears to have been at a slower rate than their introduction due to surface turbulence.

4.1.2. ZF degassing condition; gas pressure 0.0 bar, rotor speed 600 rpm

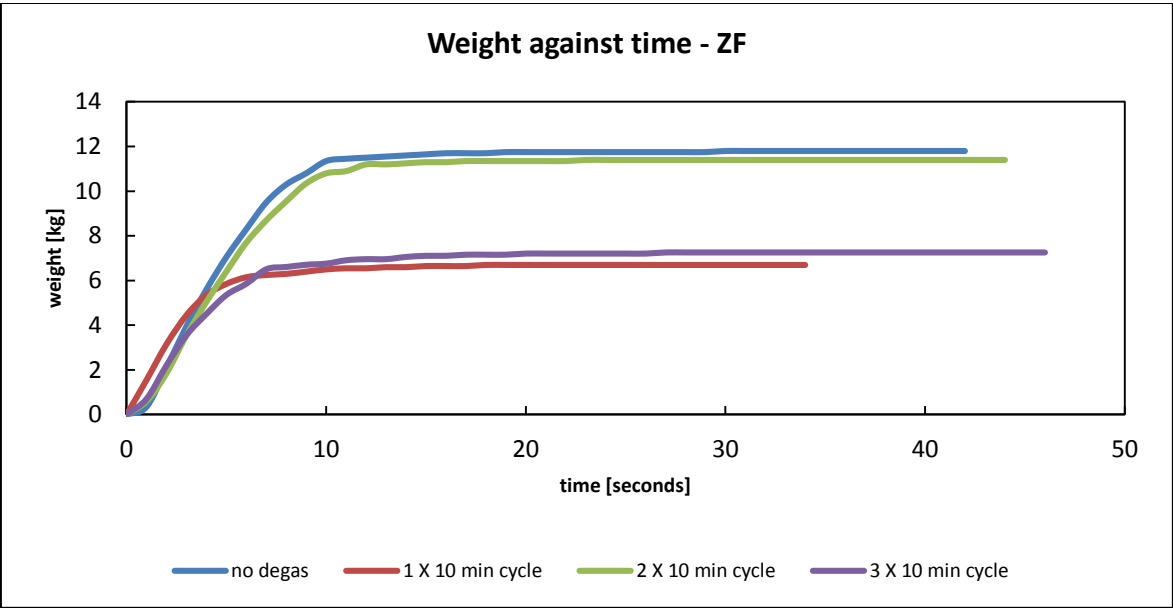


Figure 9. Weight against time - ZF.

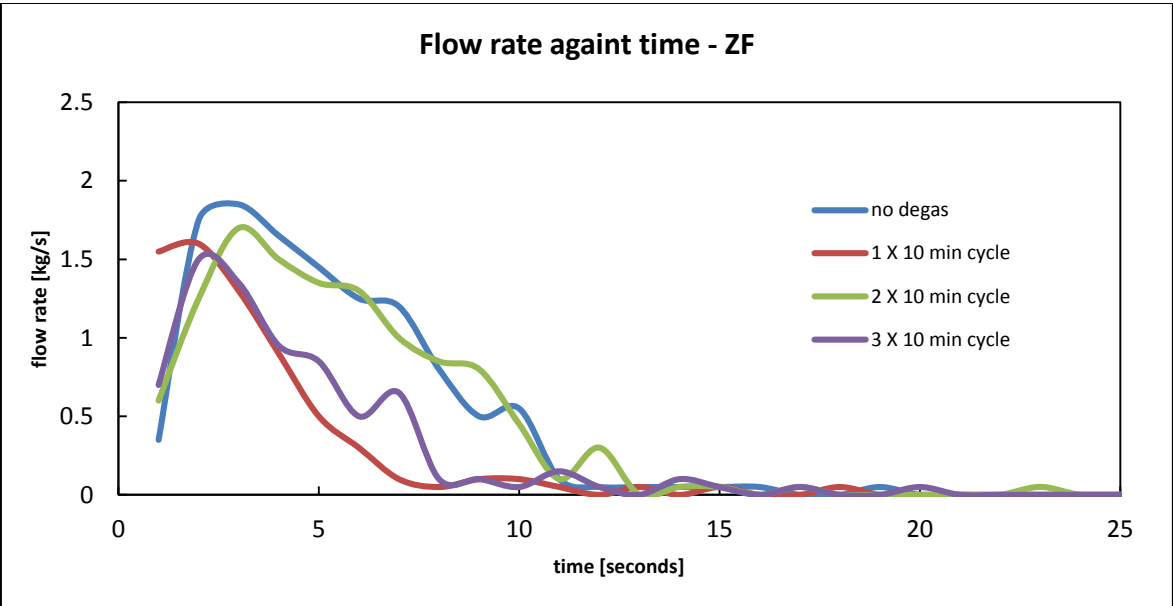


Figure 10. Flow rate against time - ZF.

The zero gas flow rate (0.0 bar gas pressure) with a fast rotor speed (600 rpm) condition exhibited varying responses to each 10 minute degassing cycle. The starting condition and the measurement after 2 cycles (20 minutes total degassing) show very similar results; in both the full sample of metal passed through the filters and the flow rates decreased at approximately the same rate. The other two readings, after 1 and 3 cycles (10 and 30 minutes total degassing time), were also very similar to each other; both samples stopped flowing through the filters at 6.7 kg and 7.25 kg respectively. The reading after the first cycle however exhibited the fastest decrease in flow rate of this condition.

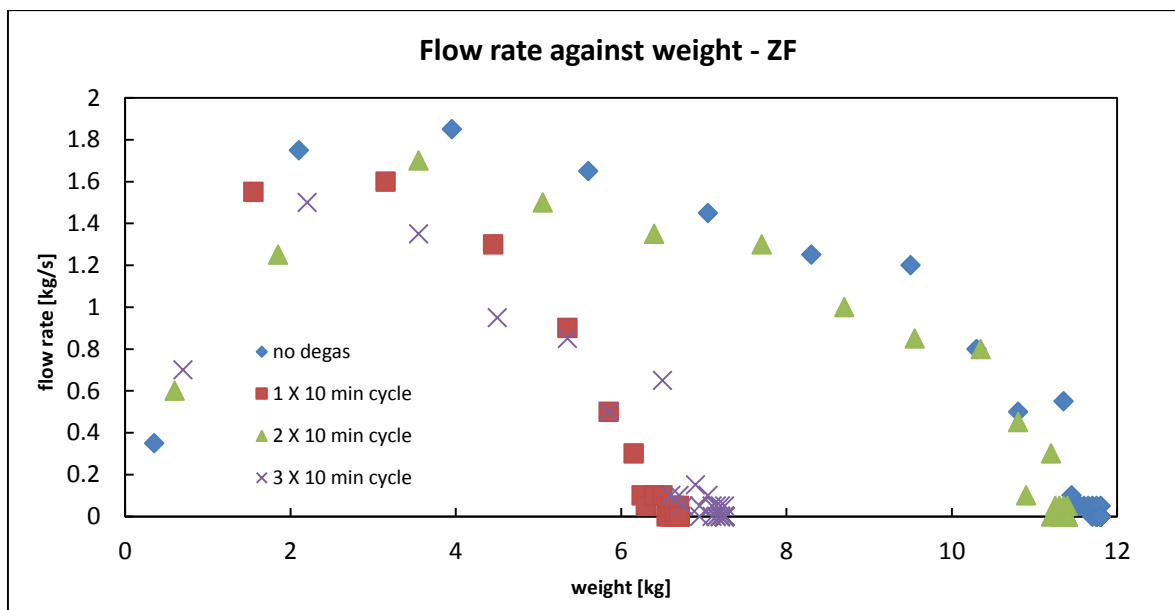


Figure 11. Flow rate against weight - ZF.

The flow rate against weight graphs shows the same pattern with the no degas and 2 x 10 min cycle showing a similar linear decrease in flow rate with weight (until the end of the sample

delivery where the flow rate drops quickly). The readings after the 1<sup>st</sup> and 3<sup>rd</sup> cycles both show a non-linear and much faster decrease in flow rate with weight.

This condition appears to be unstable. Assuming no difference in the transfer and pouring of the metal the entrainment and / or removal of films from the melt has not been consistent. In this condition there is visibly more turbulence on the surface of the melt which logically suggests a greater quantity of entrainment per time. Following this logic the improvement in flow through the filters seen after the third treatment is unexpected.

It is to be noted that there is an improvement in flow through the filters between the first and second degassing cycles suggesting that the second degassing cycle decreased the quantity of films in the melt. If this is correct then this removal has not been as a result of bubble interaction as no bubbles were passed through the melt. Removal must have happened via other mechanisms.

4.1.3. LS degassing condition; gas pressure 0.3 bar, rotor speed 120 rpm

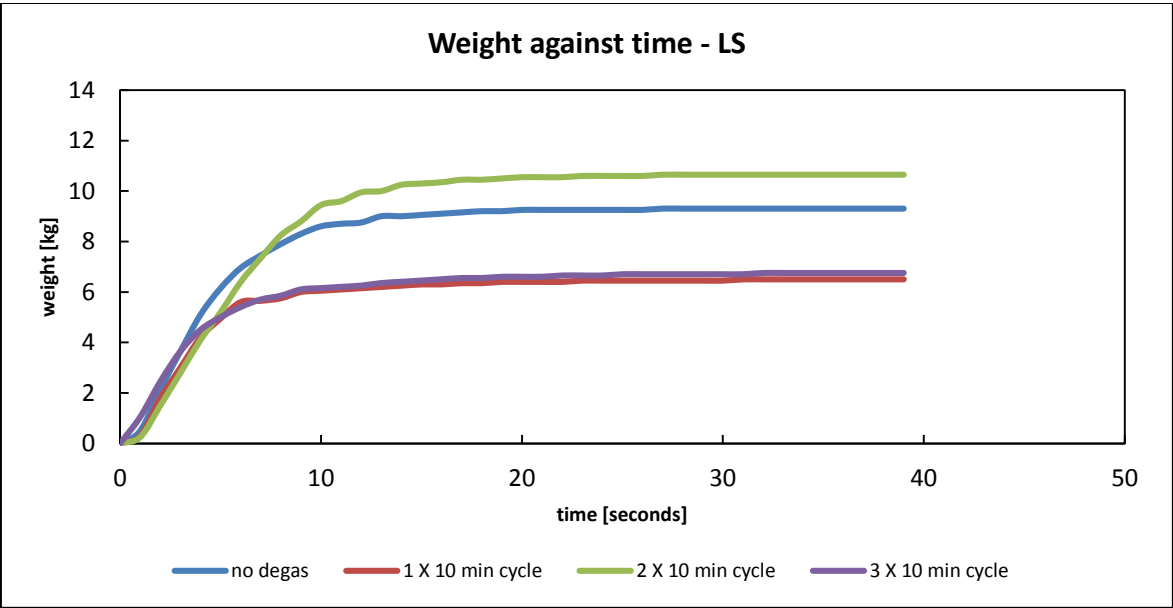


Figure 12. Weight against time - LS.

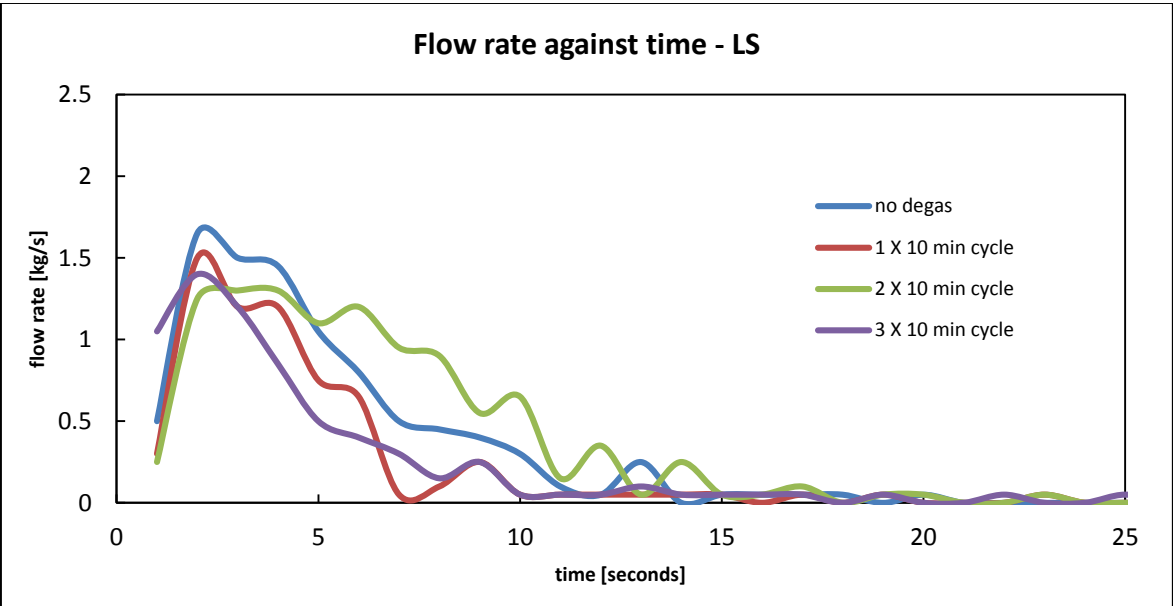


Figure 13. Flow rate against time - LS.



The low gas flow rate (0.3 bar gas pressure), slow rotor speed (120 rpm) exhibited varying responses to each 10 minute degassing cycle. As was seen in the ZF condition the initial measurement and the measurement after 2 x 10 minute cycles showed similar responses with apparent higher cleanliness levels than after the 1<sup>st</sup> and 3<sup>rd</sup> cycles. The measurement after the second cycle (20 mins total degassing time) showed the slowest decrease in flow rate indicating that the metal here was cleaner than the starting condition (although unusually this measurement had a lower maximum flow rate).

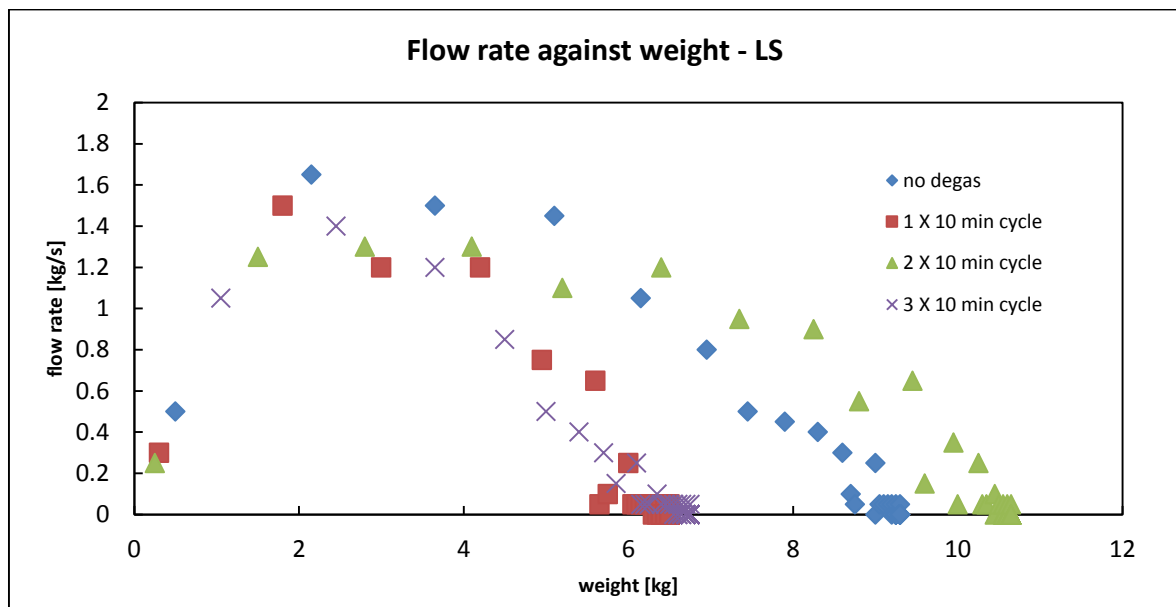


Figure 14. Flow rate against weight - LS.

The flow rate against weight graph for the LS condition also shows the separation in the measurements however no measurements appear to show a linear response.

This condition also showed visible turbulence on the melt surface, this time caused by large bubbles breaking the surface but minimal disturbance from the rotation. It is likely that this is

entraining oxide films into the melt, and as this is constant through the degassing cycles, continuous entrainment is probable. In this condition, unlike the previous conditions, ZS and ZF there is constant bubble activity in the melt which may be interacting with entrained films. Both the surface turbulence and the bubble activity are constant however in all degassing cycles so the varying response must be as a consequence of at least one additional mechanism. It is not clear from this degassing condition the contribution that either the bubbles or surface turbulence are making to the melt cleanliness however it is clear from the varying response that their contribution is less than the other mechanism(s).

The slow rotor speed in this condition will not have led to considerable bubble shearing resulting in a comparatively large bubble size and possible poor distribution through the melt. Therefore a fast removal of film from the melt would not be expected here.

4.1.4. LF degassing condition; gas pressure 0.3 bar, rotor speed 600 rpm

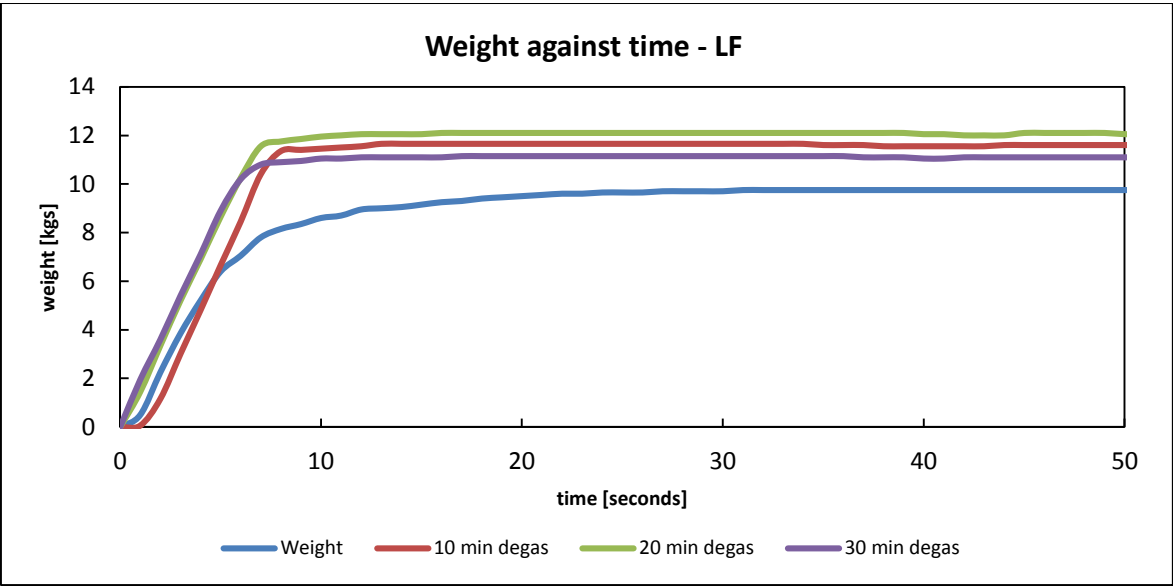


Figure 15. Weight against time - LF.

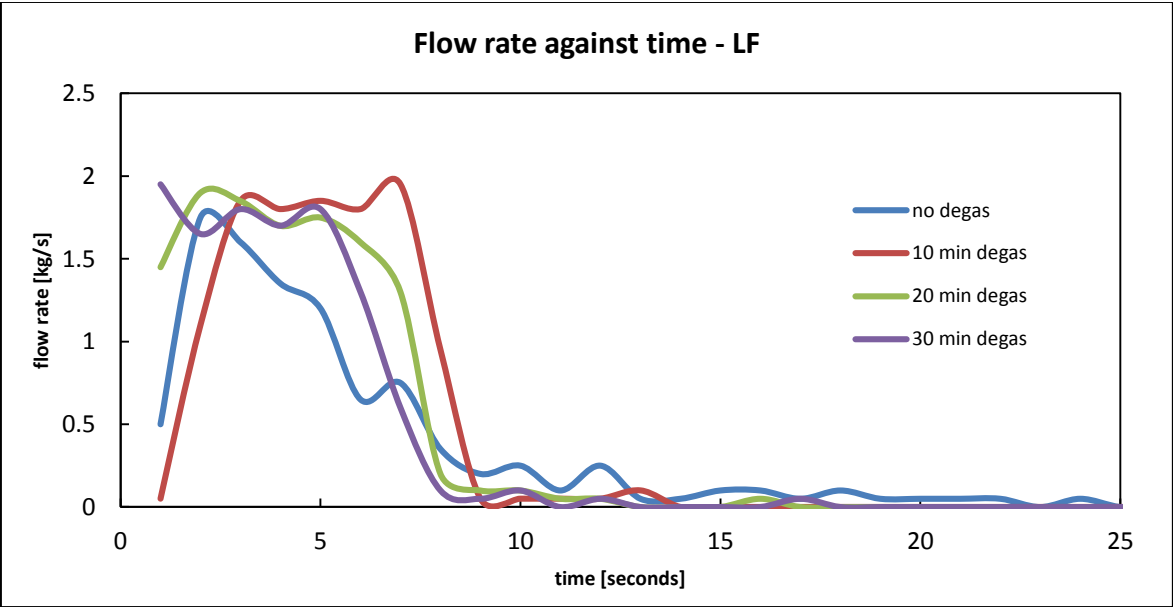


Figure 16. Flow rate against time - LF.

The low gas flow rate (0.3 bar gas pressure) with a fast rotor speed (600 rpm) condition shows a gradual decrease in flow rate with time for the initial sample, prior to any degassing suggesting a population of oxide film in the melt at the start of testing. For all of the readings taken after the degassing cycles a high flow rate of between 1.5 and 2.0 kg/second was achieved and maintained for the full sample of metal. As there was not significant decrease in flow rate as more metal passed through the filter there must be no additional resistance to flow through the filter. This indicates that no films of a size and strength to retard flow were present in the melt at the end of any of the cycles.

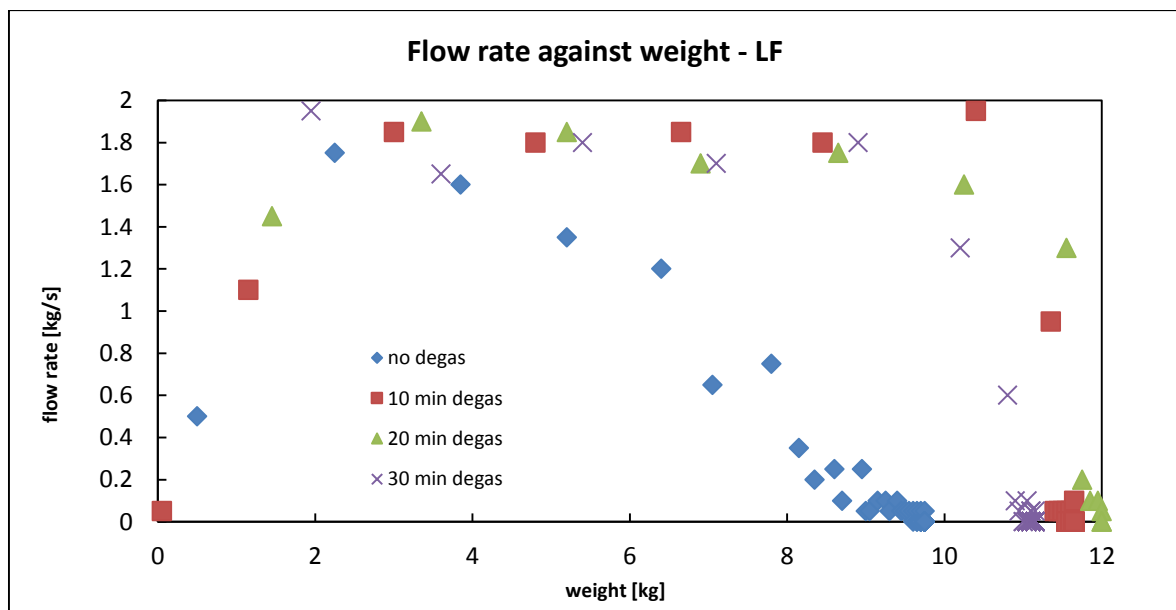


Figure 17. Flow rate against weight - LF.

The flow rate against weight graph also illustrates the same pattern. The no degas condition showed a fairly linear decrease in flow rate with weight suggesting a population of films within the melt. All subsequent measurements then show the flow rate remaining constant for all metal delivery. Although this has resulted in no 'improvement' being seen over the course of

the degassing cycles, this may indicate the theoretical maximum flow rate and therefore maximum cleanliness with regards to large oxide films.

Theoretically this degassing condition will produce the smallest bubbles out of all of the experiments in this thesis – slower gas flow rate should lead to smaller bubbles due to less gas being available and the faster rotor speed will result in greater bubble shearing which will also contribute to the smaller bubble size. Smaller bubbles could be contributing to the efficient cleaning melt in two ways. Firstly the smaller bubbles will create less turbulence at the surface of the melt when released into air leading to less entrainment of new films. Secondly they must be removing films from the melt - the turbulence alone of the fast rotor speed did not result in efficient cleaning with zero gas flow rate.

4.1.5. HS degassing condition; gas pressure 1.2 bar, rotor speed 120 rpm

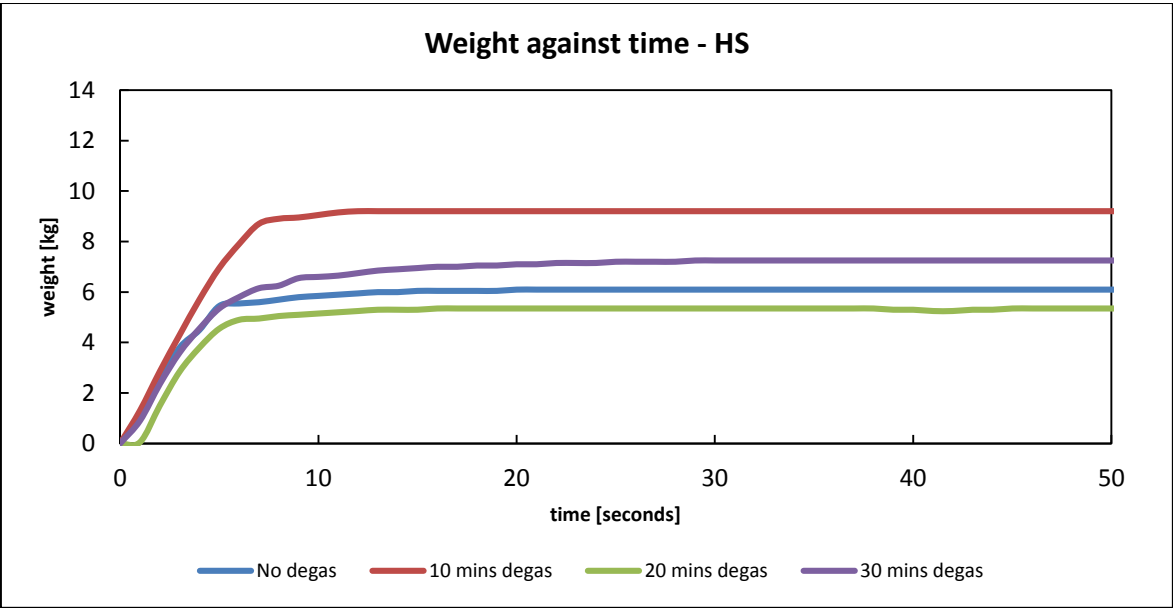


Figure 18. Weight against time - HS.

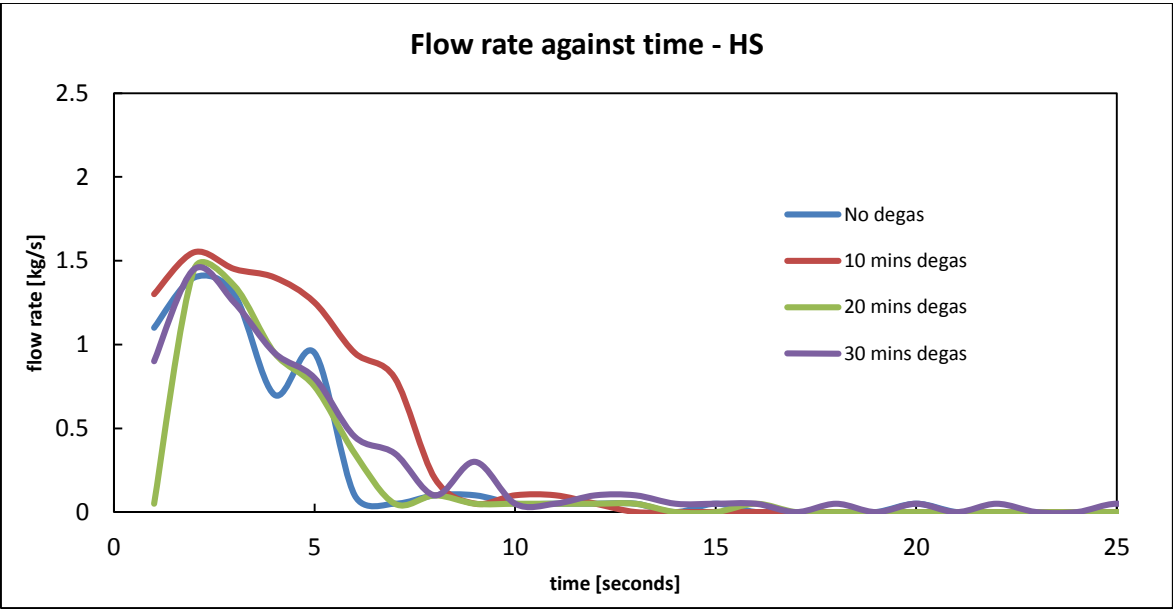


Figure 19. Flow rate against time - HS.

The high gas flow rate (1.2 bar gas pressure) with a slow rotor speed (120 rpm) condition shows varying responses to each 10 minute degassing cycle. Both increases and decreases in weight and rate of reduction of flow rate over the course of a degassing cycle are observed. The reduction in flow rate over time is not linear for the no degas and 10 mins degas conditions. This again suggests more dominant mechanisms taking place with regards to the entrainment and removal of films than the surface turbulence or bubble interaction.

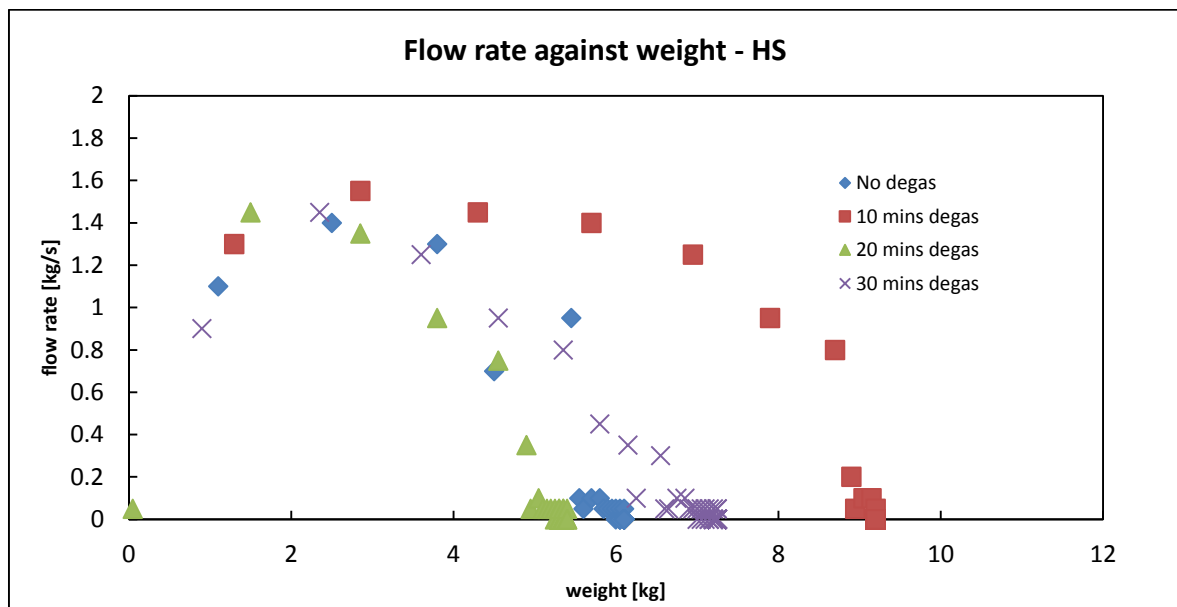


Figure 20. Flow rate against weight - HS.

The flow rate against weight graph shows only the final measurement after 30 minutes total degassing to have a linear decrease in flow rate. All other measurements show non-linear decreases.

All of the data presented for this condition shows an unpredictable response to degassing. This condition theoretically should give the largest bubble size of all the conditions tested as

both the high gas flow rate and slow rotor speed should contribute to the formation of larger bubbles. It was evident during the experiment that the large bubbles were causing a lot of turbulence on the surface of the melt which is likely to have contributed to decreasing the cleanliness of the. The bubbles may have removed oxide films from the melt however were not the dominant mechanism.



4.1.6. HF degassing condition; gas pressure 1.2 bar, rotor speed 600 rpm

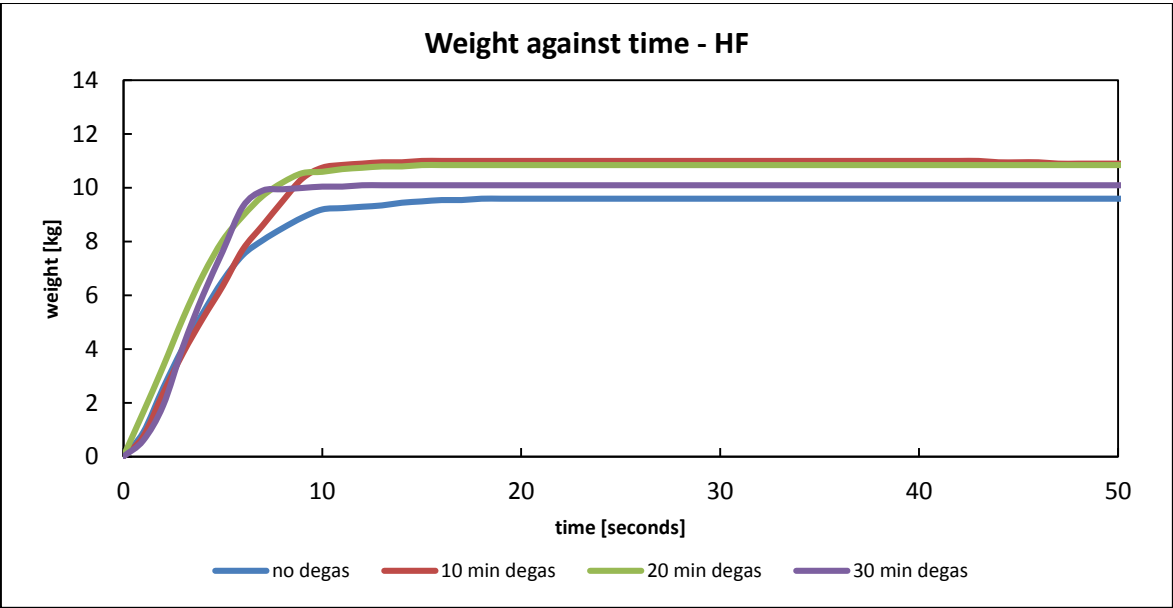


Figure 21. Weight against time - HF.

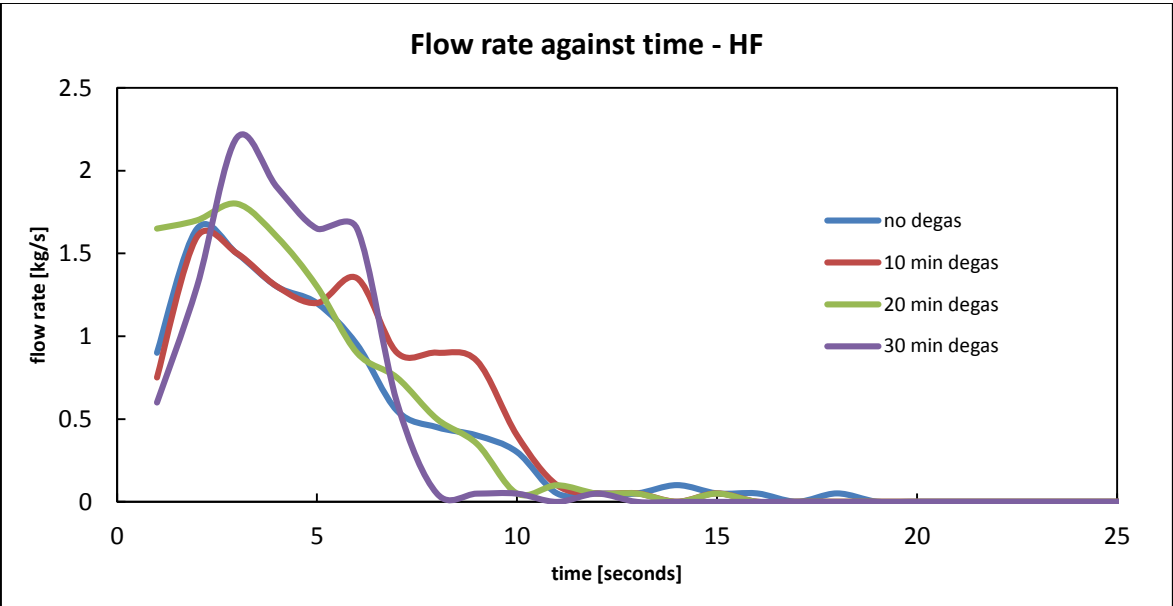


Figure 22. Flow rate against time - HF.

For high gas flow rate (1.2 bar gas pressure) with a fast rotor speed (600 rpm) condition the full metal sample has passed through the filters in all measurements. The negative gradient of the flow rate against time decreases with each degassing cycle with the final measurement showing a high flow rate for the whole sample. This suggests an increase in cleanliness for each cycle. The decrease in flow rate against time after the first and second degassing cycles indicates a population of films remaining in the melt.

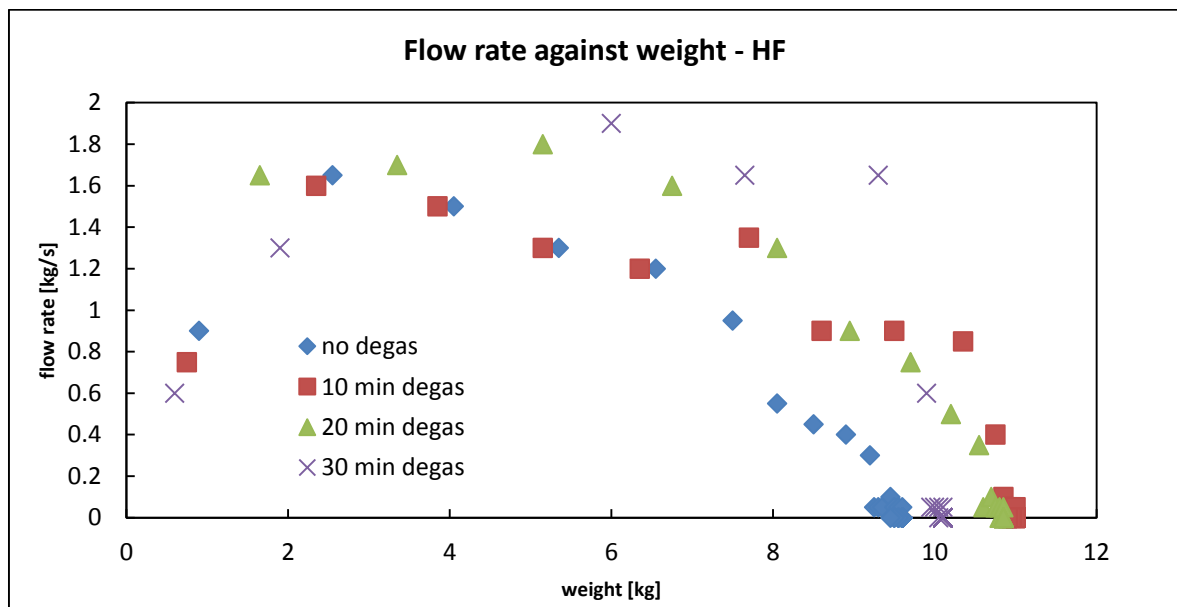


Figure 23. Flow rate against weight - HF.

The flow rate against weight graph shows the improvement in each condition slightly better than the other two graphs. The no degas and the 10 minute degas measurements decrease in flow rate at a very similar rate until approximately 6.5kg at which point the flow rate of the 10

minute measurement increases. It may be possible that this increase in flow rate could be rupture of some of the oxide films that have covered the filter.

This degassing condition (HF) theoretically will have larger bubbles than the low gas flow rate, fast rotor speed (LF) condition which appeared to exhibited a total removal filter-blocking oxide films within the first 10 minutes of degassing. The rotor speeds for the HF and LF conditions were the same therefore the gas flow rate and therefore the bubble size and distribution through the melt appear to have had an influence. If the retention of flow rate with increasing volume of metal through the filters is truly an indication of increased cleanliness then it appears that the removal of films via bubble interaction in this degassing condition is the dominant mechanism taking place.

## 4.2. Comparisons – Characterisation figure

A lot of information can be gained from the flow rate against weight graphs however it is difficult to directly compare one degassing condition to another and also the change in cleanliness per 10 minute degassing cycle for each condition. Due to this a 'characterisation figure' has been used. It is important to not over simplify large portions of data so a single figure that characterises each cleanliness test should be carefully considered and genuinely representative of cleanliness.

For the characterisation figure the portion of the flow rate against weight graph from 4 to 8 kg was assessed. This ensures that during all of this period metal delivery from the ladle was constant as the ladle held approximately 10 to 13 kg. This eliminates false readings that may have been influenced by the lack of supply of metal. It also eliminates scatter created in the first 4 kg of metal through the filter. False readings may have been gained here due to the manual pouring method and the variation in filling the bush.

The characterisation figure is defined as the area under the flow rate vs. weight curve between 4 and 8 kg [units – Kg<sup>2</sup>/s]. This figure therefore takes into account both the quantity of metal passing through the filters during this section of metal delivery and the decrease in flow rate per time that is seen in many of the samples and is likely to be a result of oxide film accumulation on the filter.

For the calculations the intercept at 4 and 8 kg assumed a straight line between the 2 adjacent data points.

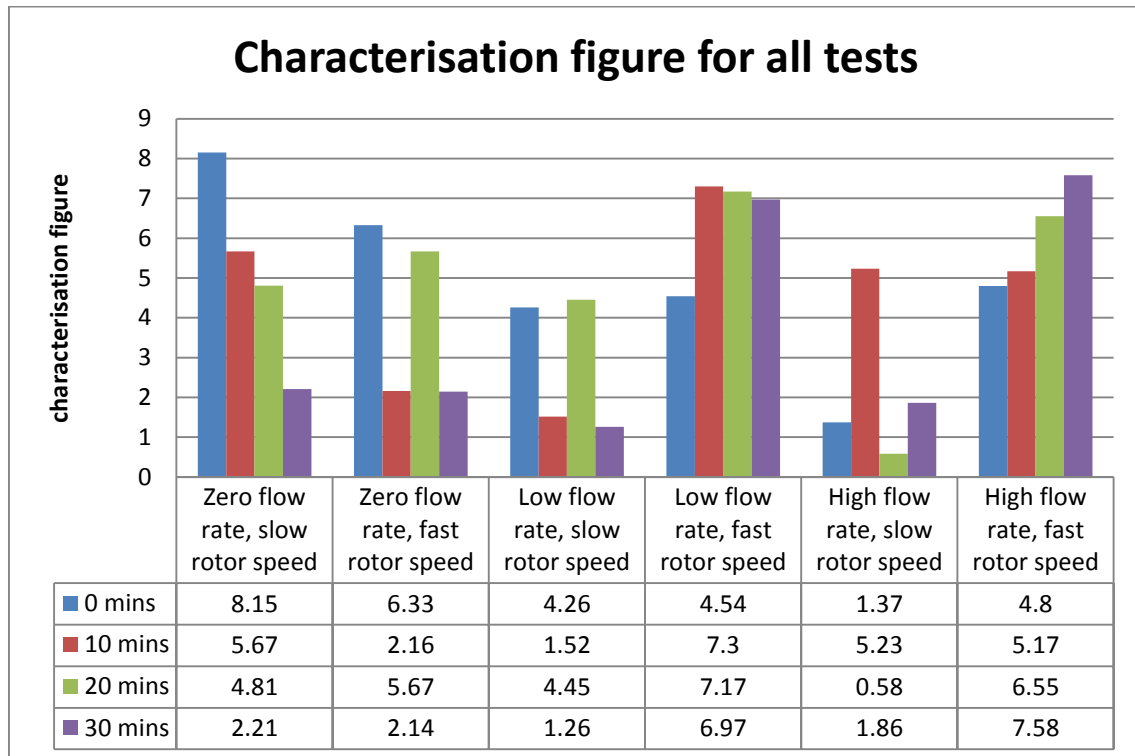


*Figure 24. Characterisation figure for all tests.*

### 4.3. Bubble – oxide film interaction

*The following discussion is written on the presumption that the data presented above is a reasonable representation of the quantity of oxide films in the melt and that films caught on or in the filter are the cause of the reductions in flow rates of aluminium that have been observed. This has been validated in section 4.3 – filter analysis.*

The characterisation figure analysis shows the only 2 conditions that have consistently improved the cleanliness are the fast rotor speeds with bubbles present. The slow rotor speed conditions and the conditions with zero gas flow rate either consistently decreased the cleanliness or show sporadic responses that do not result in good cleanliness levels. In both beneficial conditions small bubble sizes will have been produced due to the greater level of bubble shearing. This has been shown in the work of Wu et al (2007) where experiments with rotating impellers in water gave smaller bubble sizes with faster rotor speeds. It was evident on the surface of the melt that the faster rotor speed also resulted in a more even distribution of bubbles within the melt with bubbles breaking the surface in all areas whereas the slower rotor speeds resulted in bubbles only breaking the surface near the impeller. The improvement in bubble distribution through the melt may have contributed to the increased oxide film removal.

The size of the bubbles do appear to have an influence on the cleanliness of the melt as the condition with theoretically the smallest bubbles shows the fastest cleaning of the melt. Both the low and high flow rates with fast rotor speeds (LF and HF) start with a similar level of melt cleanliness. The low flow rate (LF) condition then reaches maximum cleanliness within the first cycle and then stays at this level after the subsequent cycles whereas the high flow rate condition (HF) takes 3 cycles to reach maximum cleanliness (the maximum cleanliness was

identified when the flow rate was constant until the end of metal delivery – this appears to correlate with a characterisation figure of between 7 and 8). It is unclear if both conditions are removing films at the same rate and the larger bubble size has reintroduced films at the surface resulting in slower cleaning or if the smaller bubbles do in fact remove films from the melt at a faster rate.

It can be concluded however that the purge bubbles are having a large effect in removing oxide films as both the conditions where a zero gas flow rate was used did not clean the metal and in most instances decreased the cleanliness. This shows that turbulence and transport due to flow patterns in the melt is not effective at removing oxide films whereas bubbles are. It is fair to assume from this that there is some interaction / collision between the bubbles and the oxide films. As identified in the literature review pure argon will not chemically react with particles / films. This means that some sort of mechanical lifting of the film by the bubbles is most likely taking place.

When comparing particles / inclusions to oxide films their difference in shape is most notable. Oxide films are likely to occupy more cross sectional area when compared to most inclusions. With the presence of many small bubbles this could increase the likelihood of bubble – film collision. Oxide films often become crumpled or deformed. It may be the case that bubbles could become lodged in the crevices of films resulting in mechanical but not chemical attachment. If this were to be the case then a smaller bubble size would increase the likelihood of this sort of attachment as the bubble would physically fit into the crevices of the film whereas larger bubbles may not. This mechanism could be responsible for the increased oxide film removal with the presence of smaller bubbles.

It must also be considered that the disturbance on the surface of the melt in the conditions with larger bubbles is greater. This could be leading to the formation of more oxide films that could become entrained into the melt via the stirring action of the impeller, counteracting the cleaning effect of the bubbles.

It is shown in the literature review that larger bubbles have the most potential at removing particles however no notable difference in  $\text{TiB}_2$  particle removal can be observed between the degassing conditions with different bubble sizes. As seen in the work by Warke et al it is likely that the size of the  $\text{TiB}_2$  particles in the A20X system are too small to be effected. The use of pure argon as the purge gas also avoids the possibility of chemical wetting between the bubbles and the  $\text{TiB}_2$  particles. This is advantageous as it allows the degassing cycle to be designed focusing on the removal of oxide films.

The level of hydrogen removal however could limit how low of a flow rate is used. Due to the high melt holding temperature of the A20X system a sufficient level of hydrogen removal is shown to be difficult to achieve. Although there is no notable difference in gas removal between the different conditions presented in this thesis, theoretically it still remains that a higher level of purge gas will be more effective at removing hydrogen.



## 4.4. Unstable degassing conditions – possible causes

The degassing conditions ZF, LS and HS have exhibited varying responses to each degassing cycle, sometimes showing an apparent removal of films and sometimes showing an increase in films (assuming the flow rates in the data presented above are dominated by oxide film deposits on the filters). It is not clear why this is the case but the following scenarios may be likely candidates:

Sporadic mechanisms that remove films in bulk which occur less than once per 10 minute degassing cycle. Agglomeration of oxide films may be a culprit. With the turbulence induced by the rotation of the degassing impeller it is increasingly likely that a higher concentration of films will lead to film-film interaction or contact. Potentially agglomeration of films may change their effective density causing them to float out faster than single films. Alternatively the size of the agglomeration may change their coefficient of drag when liquid metal moves by them, causing them to reach the crucible walls or melt surface faster than single films.

Another scenario is that agglomerations of films are more likely to interact with or trap bubbles due to their larger cross-sectional area which may carry the agglomeration to the surface of the melt faster than individual films. This set of experiments is incapable of identifying if these mechanisms lead to the unpredictable results observed.

It may be the case that the production or entrainment of oxide films is inconsistent in the ZF, LS and HS conditions. From observation of the melt this seems unlikely but would be difficult to prove or quantify. A larger sample of experiments perhaps with a shorter degassing time per cycle may help to identify if this is the case.

In the literature review it is highlighted that different types, shapes and thicknesses of oxide films may be present. This may have led to unpredictable results as the different films present may have different effects on the flow rate when caught on the filter. It is likely that different thicknesses of films have different strengths – they may initially bridge filter pores and then rupture – it is difficult to identify if and when this occurs and what the effect would be on the bulk aluminium flow but could be a candidate mechanism for the sporadic results.

## 4.5. Experimental errors

Finally the unpredictable results may be down to inaccuracies in the experiment. There may be error which leads to a variation in the density of oxide films and also there may be error in the actual measurement. The holding time of the molten metal is likely to produce oxide films of different thicknesses and strengths (as discussed in the literature review). The holding time between degassing conditions was controlled however the effective holding time of returns that were used was not controlled – differing thickness films may have formed on returns when they originally solidified.

Metal temperature was controlled during the experiment however small variations may have introduced errors as they will have altered the rate of formation of oxide films. In addition, all temperature measurements were in the melting pot – it is unknown how much temperature variation was introduced during the transfer of the metal to the pouring bush. This could have also altered the strength of the oxide films and potentially changed their behaviour on the filters.

The manual transfer of the metal from the melt to the mould and the pouring of the metal into the bush is unlikely to be completely consistent in terms of oxide film entrainment. Repeats of the experiment would help to identify how much scatter is introduced due to the experimental procedure itself. Without this it is difficult to identify how repeatable the experimental procedure is.

In the measurement of the flow rate itself there may be errors. The weight was measured downstream of the filters therefore errors may be created due to inconsistent flow between the filters and the bath placed on the scales.

## 6. Filter Analysis

To confirm that the characterization figure is representative of the cleanliness of the melt the front face of the filters for LF were analysed. The 2 conditions analysed were the starting condition before any degassing and condition after 1 10 minute degassing cycle. 1 filter from each was analysed. A single section / plane was examined over the full height of the filter face. The characterization figures suggest a large increase in cleanliness during the course of this first 10 minute degassing cycle.

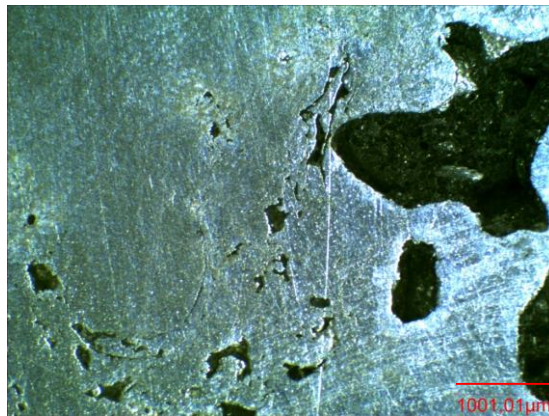


*Figure 25. The front face of the first filter, section down the centreline for the starting condition - no degassing in the low gas flow rate, high rotor speed experiment. This exhibits large amounts of oxide films spanning the front face of the filter. The direction of the metal flow here is from left to right.*

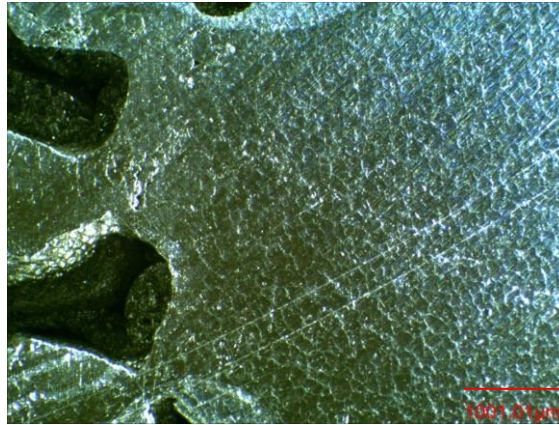


*Figure 26. The front face of the first filter, sectioned down the centreline for the low gas flow rate, high rotor speed condition after the first 10 minute degassing cycle. This condition shows considerably less oxide films that have been caught by the front face of the filter. The direction of metal flow here is from right to left.*

The results of the filter analysis show that the characterization figure is a good representation of the cleanliness of the melt at the time of testing.

## 4.7. TiB<sub>2</sub> removal

Boron levels which are directly proportional to TiB<sub>2</sub> levels were measured and the results are shown below in *table 6*:

*Table 6. Boron contents [wt%] for all conditions.*

TIME	ZS – BORON	ZF – BORON	LS – BORON	LF – BORON	HS – BORON	HF – BORON
[MINUTES]	[WT%]	[WT%]	[WT%]	[WT%]	[WT%]	[WT%]
<b>0</b>	0.022	0.043	0.193	1.21	1.117	0.642
<b>10</b>	1.151	1.32	1.165	1.307	1.106	1.113
<b>20</b>	1.207	1.366	1.159	1.18	1.128	1.048
<b>30</b>	1.225	1.265	1.154	1.192	1.172	1.063

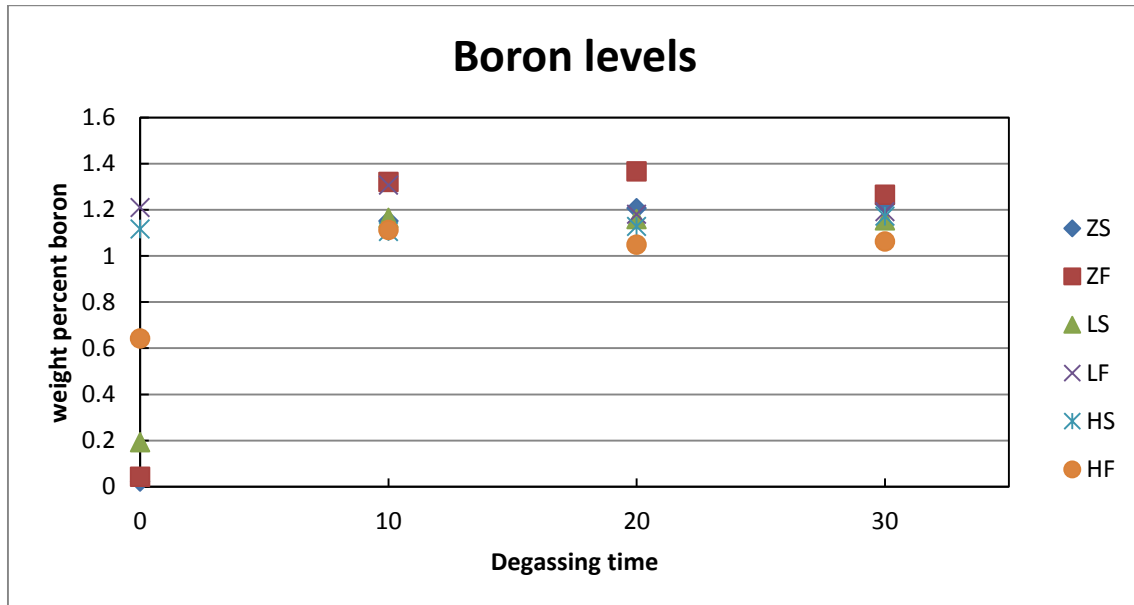


Figure 27. Boron levels for all conditions.

Some very low levels of boron were found only in the samples taken before any degassing cycles. No notable trends are visible that suggest removal of  $\text{TiB}_2$  particles from the data points at 10, 20 and 30 minutes degassing time from any of degassing conditions.

## 4.8. Density index readings (DI)

High gas needs to be avoided as it reduces the strength and ductility of the material. Eisaabadi et al (2012) clearly illustrates this and shows a reduction in both UTS and elongation when hydrogen content was increased from 0.11 ml/100g to 0.44 ml/100g in an A356-T6 material.

The target is a DI of 1.0 or less which in practice has shown to reliably give high integrity castings. Haberl et al (2009) states that a density index reading of 1.0 corresponds with a hydrogen content of 0.1mL / 100g of aluminium therefore this is in line with Eisaabadi's illustration of improved mechanical properties at approximately this level.

Density index reading were taken immediately prior to pouring for all flow measurements and the results are show in *table 7* below:

*Table 7. Density index (DI) values for all conditions.*

TIME [MINUTES]	ZS	ZF	LS	LF	HS	HF
0	0.3	14	3.8	12.7	2.7	4.1
10	3.9	13.1	2.7	1.8	2.1	2
20	4.4	12.5	0.7	1.4	1.7	0.7
30	5.8	14.4	1.8	0.9	2.1	0.9



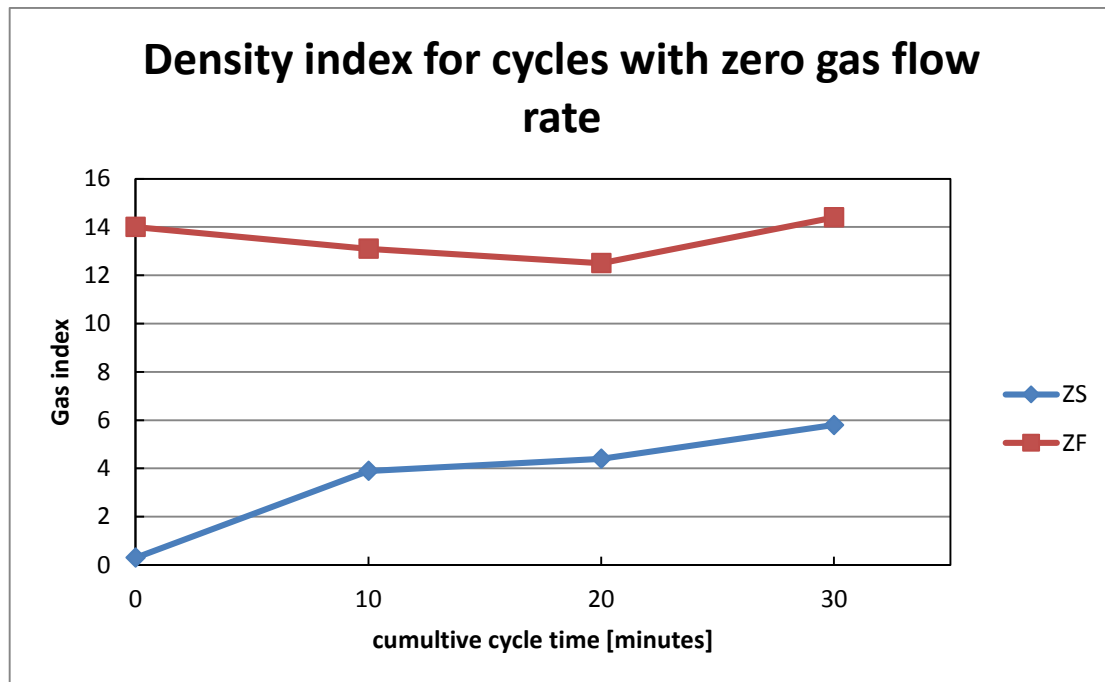


Figure 28. Density index for cycles with zero gas flow rate.

The conditions with zero gas flow rate, as expected did not achieve acceptable gas levels. The starting gas level for the slow and fast rotor speeds were vastly different however the slow rotor speed gas level increased after the first cycle to give a DI of 3.9 – higher than acceptable. The DI has then continued to increase with each subsequent cycle. The fast rotor speed has only caused an increase in gas with the final cycle. The level on all readings however is very high and can be considered saturated.

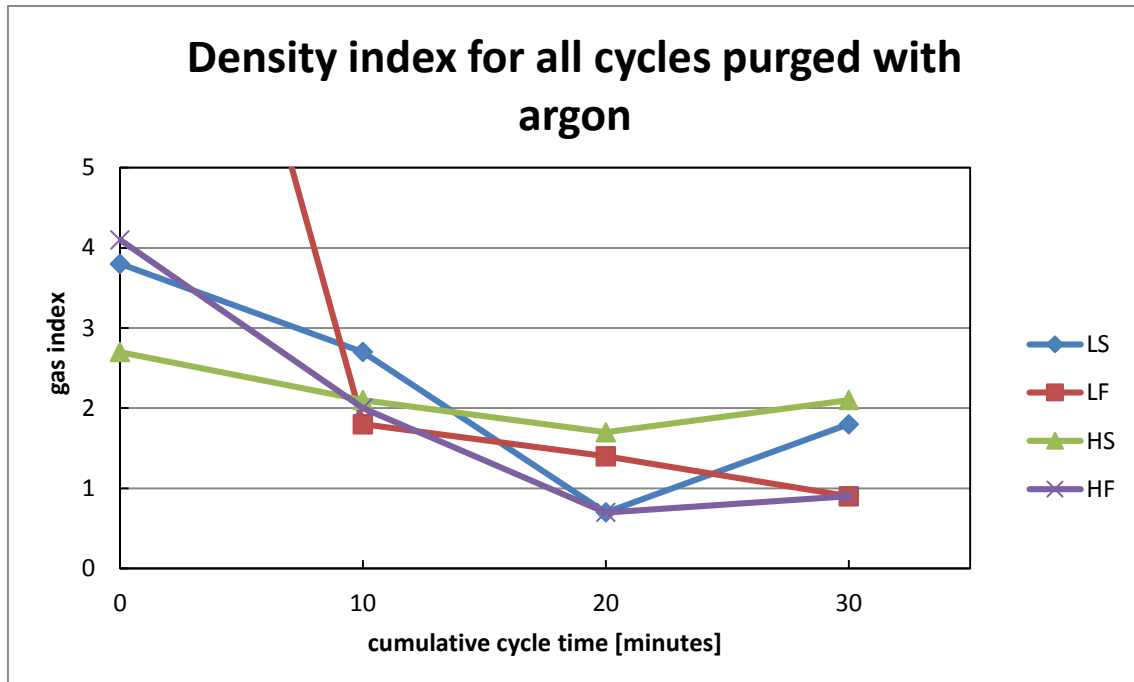


Figure 29. Density index for all cycles purged with argon.

The DIs for the cycles that received an argon purge all had different starting levels, most notably the LF condition which had a starting gas index of 12.7. From experience all ‘traditional’ foundry alloys which have a melt holding temperature of 750°C or less will achieve a DI of well below 1.0 with a 10 minute degassing cycle at optimum settings. For this A20X system with a melt holding temperature of 800°C no cycle has achieved a DI below 1.0 after the first 10 minute cycle. It is likely that the higher melt temperature has caused a high level of gas pick up at the surface of the melt which counteracts the loss of hydrogen through the degassing process.

The different degassing processes do not appear to achieve vastly different levels of gas removal. The only distinction can be seen in the HS condition which created large amounts of disturbance on the melt surface due to the large bubble size which could be responsible for gas introduction.

## 5. Conclusions

1. Argon purge bubbles passed through an A20X melt do have the potential to remove oxide films.
2. Argon purge bubbles will not remove significant amounts of  $\text{TiB}_2$  particles from an A20X melt.
3. Fast impeller rotation speeds – 600 rpm in the case of the experiments within this thesis – are required for efficient cleaning of an A20X melt.
4. For the fast rotor speed (600 rpm) conditions the low gas flow rate given by a pressure of 0.3 bar appeared to remove oxide films faster than the high flow rate given by 1.2 bar pressure. The lower flow rate will have produced smaller bubbles therefore it appears likely that smaller argon bubbles are more effective at reducing the amount of oxide films in an A20X melt either by more efficient removal and / or reduced re-entrainment of films at the melt surface.

## 6. References

1. Campbell J. (2003) **Castings**, pub Butterworth-Heinemann Ltd, Oxford, UK, pp. 212 - 217

2. Campbell J. (2003) **Castings**, pub Butterworth-Heinemann Ltd, Oxford, UK, pp. 267

3. Campbell J. (2003) **Castings**, pub Butterworth-Heinemann Ltd, Oxford, UK, pp. 132

4. Campbell J. (2003) **Castings**, pub Butterworth-Heinemann Ltd, Oxford, UK, pp. 2 - 8

5. B. S. Murty, S. A. Kori, M. Chakraborty (2002)

Grain refinement of aluminium and its alloys by heterogeneous nucleation and alloying.

**International Materials Reviews**, Vol. 47, pp 3 - 29

6. T. E. Quested (2004)

Understanding mechanisms of grain refinement of aluminium alloys by inoculation

**Materials Science and Technology**, Vol. 20, pp 1357 - 1369

7. R. R. Roy, T. A. Utigard, C. Dupuis (2001)

Inclusion removal kinetics during chlorine fluxing of molten aluminum

**Light Metals**, 2001, pp 991 – 997

8. V. S. Warke, S. Shankar, M. M. Makhlouf

Mathematical modelling and computer simulation of molten aluminum cleansing by the rotating impeller degasser Part II. Removal of hydrogen gas and solid particles

**Journal of Materials Processing Technology**, Vol. 168, pp 119 - 126

9. V. S. Warke, G. Tryggvason, M. M. Makhlouf

Mathematical modelling and computer simulation of molten aluminum cleansing by the rotating impeller degasser Part I. Fluid flow

**Journal of Materials Processing Technology**, Vol. 168, pp 112 - 118

10. P. L. Schaffer, A. K Dahle (2009)

The effect of degassing on grain refinement in commercial purity aluminum

**Metallurgical and Materials Transactions A**, Vol. 40A, pp 481 - 485

11. D. Hewitt, D. Fornasiero, J. Ralston (1994)

Bubble particle attachment efficiency

**Minerals Engineering**, Vol. 7, pp 657 – 665

12. A. V. Nguyen, J. Ralston, H. J. Schulze (1998)

On modelling of bubble – particle attachment probability in flotation

**International Journal of Mineral Processing**, Vol. 53, pp 225 – 249

13. B. Pyke, D. Fornasiero, J. Ralston (2003)

Bubble particle heterocoagulation under turbulent conditions

**Journal of Colloid and Interface Science**, Vol. 265, pp 141 – 151

14. B. Shahbazi, B. Rezai, S. M. Javad Koleini (2010)

Bubble-particle collision and attachment probability on fine particles flotation

**Chemical Engineering and Processing**, Vol. 49, pp 622 – 627

15. J. A. Ramirez, A. Zinchenko, M. Loewenberg, R. H. Davis (1999)

The flotation rates of fine spherical particles under Brownian and convective motion

**Chemical Engineering Science**, Vol. 54, pp 149 – 157

16. C. Celik, D. Dautre (1989)

Theoretical and experimental investigation of furnace chlorine fluxing

**Light Metals**, 1989, pp 793 – 800

17. R. Wu, D. Shu, J Wang (2007)

Flow field and gas-bubble size analysis in water model for the process of aluminum melt degassing by particle image velocimetry

**Materials Science Forum**, Vol. 546 – 549, pp 1087 – 1092

18. J. Forde. **Personal communication**. (2011)

19. D.S. Kumar, T. Rajendra, R. Prasad, A. Sarkar, M. Ranjan (2009)

Forced flotation of inclusions in tundish

**Iron and Steelmaking**, Vol. 6, pp 470 – 475

20. L. Zhang, S. Taniguchi (2000)

Fundamentals of inclusion removal from liquid steel by bubble flotation

**International Materials Reviews**, Vol. 45, pp 59 – 82

21. A. V. Nguyen (1998)

Particle-bubble encounter probability with mobile bubble surfaces

**International Journal of Mineral Processing**, Vol. 55, pp 73 – 86

22. K. Haberl, P. Schumacher, G. Geier, B. Stauder (2009)

Characterization of the melt quality and impurity content of an Lm25 alloy

**Metallurgical and Materials Transactions B**, Vol. 40B, pp 812 – 821

23. B. G. Eisaabadi, P. Davami, N Varahram, S. K. Kim (2012)

On the effect of hydrogen and Fe on reproducibility of tensile properties in cast Al-Si-Mg alloys

**Materials Science and Engineering A**, Vol. 565, pp 278 - 284

24. P.S. Mohanty, J.E. Gruzleski (1994)

Mechanism of grain refinement in aluminium

**Acta Metallurgica et Materialia**, Vol. 43, pp 2001 – 2012



25. P. L. Schaffer, A. K. Dahle (2005)

Settling behaviour of different grain refiners in aluminium

Materials Science and Engineering: A, Vol. 413-414, pp 373 – 378

26. Campbell J. (2011) **Complete casting handbook**, pub Butterworth-Heinemann Ltd, Oxford,

UK, pp. 892 - 896

27. X. Dai, X. Yang, J Campbell, J. Wood (2002)

Effects of runner system design on the mechanical strength of Al-7Si-Mg alloy castings

**Materials Science and engineering: A**, Vol. 354, pp 315 - 325

28. R. Gopalan, Prabhu, K. Narayan (2011)

Oxide bifilms in aluminium alloy castings - a review

Materials Science and Technology, Vol. 27, pp 1757 - 1769